

# Optimal coordinated operation of a multi-energy community considering interactions between energy storage and conversion devices



Xuezhi Liu<sup>a,b</sup>, Zheng Yan<sup>a,b</sup>, Jianzhong Wu<sup>c,\*</sup>

<sup>a</sup> School of Electronic Information and Electrical Engineering, Shanghai Jiao Tong University, Shanghai, China

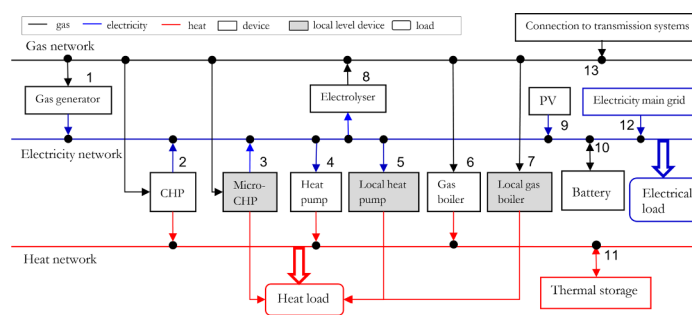
<sup>b</sup> Key Laboratory of Control of Power Transmission and Transformation of Ministry of Education, Shanghai Jiao Tong University, Shanghai, China

<sup>c</sup> School of Engineering, Cardiff University, Queen's Buildings, The Parade, Cardiff CF24 3AA, UK

## HIGHLIGHTS

- A comprehensive set of energy storage and conversion devices were modelled.
- Conversion devices were mapped to multi-network energy flows using matrices.
- Energy storage and conversion devices were decomposed and sequentially optimised.
- Interactions between multi-energy network operation limits were demonstrated.
- Impact of energy conversion devices on PV-battery systems was investigated.

## GRAPHICAL ABSTRACT



## ARTICLE INFO

### Keywords:

PV-battery systems  
Energy conversion devices  
Multi-energy communities  
Optimal operation  
Optimization  
Energy system integration

## ABSTRACT

An optimal coordinated operation model of comprehensive energy storage and conversion devices was built by considering interdependency in a multi-vector energy community, to achieve an overall optimum. The model determined the storage size, the operation strategies of energy storage and conversion devices and scenario analysis was further conducted. The proposed sequential method solved the complex mixed-integer nonlinear programming (MINLP) problem by decomposing the multi-energy system into a subsystem of conversion devices and a PV-battery subsystem, which reduced the computation complexity. Firstly, electricity, heat and gas networks were modelled in an integrated manner and with a suitable level of detail for operational purposes. The integrated electrical-hydraulic-thermal-gas flow equations imposed by multi-energy networks were formulated as equality constraints in the optimization. The optimal operation of conversion technologies with increasing net-load variability on the consumer load profiles was determined. Secondly, the design and operation of PV-battery systems was investigated to provide economic incentives for storage owners. The total costs, the self-consumption ratio (SCR), the internal return rate (IRR) of PV-battery systems were calculated. In scenario analysis, interactions between multi-energy network operation limits as well as the impact of energy conversion devices on PV-battery systems were demonstrated. It showed that the option of Combined Heat and Power (CHP) was advantageous without considering PV-battery systems using 2016 financial data. However, considering the profit of PV-battery systems and the declining grid electricity carbon intensity, the option of heat pumps was advantageous and may be a favorable option in the long term.

\* Corresponding author.

E-mail addresses: [liuxz@sjtu.edu.cn](mailto:liuxz@sjtu.edu.cn) (X. Liu), [yanz@sjtu.edu.cn](mailto:yanz@sjtu.edu.cn) (Z. Yan), [wuj5@cardiff.ac.uk](mailto:wuj5@cardiff.ac.uk) (J. Wu).

<https://doi.org/10.1016/j.apenergy.2019.04.106>

Received 10 February 2019; Received in revised form 23 March 2019; Accepted 16 April 2019

Available online 24 April 2019

0306-2619/© 2019 Published by Elsevier Ltd.

**Nomenclature****Acronyms**

PV	photovoltaic
BESS	battery energy storage systems
PVB	PV-battery systems
CHP	Combined Heat and Power
CAPEX	capital expenditure
OPEX	operating expenditure
IRR	internal return rate
SCR	self-consumption ratio
SSR	self-sufficiency ratio
SOC	state of charge
TOU	time-of-use

**Variables**

$V$	voltage (V)
$\theta$	voltage angle (rad)
$P$	electrical real power (MW <sub>e</sub> )
$Q$	electrical reactive power (MVar)
$\Phi$	heat power (MW <sub>th</sub> )
$\dot{m}$	mass flow rate within each pipe (kg/s) in heat networks
$T_s$	supply temperature at a node in the supply network (°C)
$T_r$	return temperature at a node after mixing in the return network (°C)
$E^{out}$	matrix of end-use demand (e.g., electrical power and heat power) at the conversion components
$E^{in}$	matrix of input electrical power and gas flow at the conversion components
$\mathcal{H}$	efficiency matrix of conversion devices
$\mathbf{M}$	permutation matrix
$P_{PV}$	electric power generated from PV (MW)
$P_{PV \rightarrow load}$	electric power supplied to the load from PV (MW)
$P_{PV \rightarrow BESS}$	electric power charging to the battery from PV (MW)

$P_{PV \rightarrow grid}$	electric power exported to the grid from PV (MW)
$P_{BESS}^{charge}$	maximum rate at which the battery device consumed electricity when recharging (MW)
$P_{BESS}^{discharge}$	maximum rate at which the battery device generated electricity when discharging (MW)
$P_{BESS}^{rated}$	rated power of the battery inverter (MW)
$E_{BESS}^{rated}$	rated storage capacity of the battery (MWh)
$P_{PV}^{rated}$	rated peak power of the PV system (MW)
$P_{import}$	imported grid electric power (MW)
$P_{grid}$	grid electric power to the load (MW)
$P_{import}^{limit}$	limit of imported electric power from the main grid
$P_{export}^{limit}$	limit of exported electric power to the main grid
$C_{total}$	total lifetime annualized cost
$C_{OPEX}$	annual operating expenditure (OPEX)
$C_{CAPEX}$	up-front capital expenditure (CAPEX) of system devices
$C_{O\&M}$	operating and maintenance costs of devices (O&M cost)
$L F_n$	levelised factor over $n$ years
$C_e$	electricity spot price (£/MWh)
$C_g$	natural gas price (£/MWh)
$C_{carbon}$	carbon price (£/tonne)
$C_{BESS}^E$	energy-capacity-determined cost for a battery (£/MWh)
$C_{BESS}^P$	power-capacity-determined cost for a battery (£/MW)
$C_{PV}^{CAPEX}$	capital cost of a PV panel (£/MW)
$C_{PV}^{export}$	PV export feed-in tariff (£/MWh)
$C_{PV}^{subsidy}$	subsidy price of electricity generated from PV (£/MWh)
$\xi$	carbon footprints (g <sub>CO2</sub> /kWh)
$v_g$	natural gas flow rate (m <sup>3</sup> /h)
$p$	gas pressure at each node (bar)

**Subscripts and superscripts**

$e$	electricity
$h$	heat
$g$	gas
con	conversion device

**1. Introduction**

Multi-vector energy systems considering electricity, gas, heat, cooling, hydrogen and other energy vector synergies, contribute to the local energy consumption of renewable energy and improve energy system flexibility [1]. The design and operation of the multi-vector energy system is to identify the optimal combination of energy supply, conversion and storage technologies as well as the network infrastructure required to meet the estimated energy demand and its future evolution. Integrated design and operation of multi-energy systems is beneficial compared to the independent development practiced by individual sectors today, since it takes into account synergies between the different energy vectors, which will facilitate an increasing penetration of renewable energy [2,3].

Energy storage systems have been proposed as a means of bridging gaps in renewable energy output on a range of timescales. The use of battery energy storage systems (BESS) in combination with PV systems is expected to become a widely applied energy storage solution for residences [4] and communities [5]. The benefit of the PV-battery system was to shift off-peak electricity, consume or shift surplus PV electricity. The battery sizing is a key part of the PV-battery system design process, given that the profitability of the battery is affected by its size. The selection of the optimal battery size involves a trade-off between the battery capacity and price [6] as well as network constraints [7]. There is an extensive literature on BESS charge/discharge scheduling for residential buildings that are coupled with solar PV systems [8]. Self-consumption becomes an important driver of solar

adoption in markets around the world, which describes how much of the locally generated electricity was consumed on-site (both for matching instantaneous demand as well as for storing) [9]. McKenna et al.'s study focussed on average levels of PV self-consumption in the UK, but in the absence of 'enabling technologies' such as batteries or electric vehicles [9]. Linssen et al. investigated the influence of the temporal resolution of the input load and PV profiles on the self-consumption for a PV-battery system [10]. For commercial buildings, Mariaud et al. investigated the integrated optimization of photovoltaic and battery storage systems [11]. Critical aspects which could affect energy storage revenue which have not been examined include significant changes in patterns of demand as a result of wide spread uptake of electric vehicles, heat pumps or demand side response. The impact of heat pumps on the levelised cost and the profitability of community batteries was simply conducted by McKenna et al. [12], but without PV-battery coupling and detailed network operational studies. Battery storage in residential areas to alleviate the impacts of heat pumps was conducted by Pimm et al. [13], but without further cost benefit analysis. Yu et al. investigated the optimal sizing of energy storage system at building level with Combined Heat and Power (CHP) [14], without considering PV or heat pumps.

Regarding energy conversion devices (such as gas-fired CHP, gas boilers and heat pumps), Mashayekh et al. proposed a mixed integer linear programming approach for optimal distributed energy resource portfolio, sizing, and placement in multi-energy microgrids [15]. The optimal scheduling of smart homes' energy consumption was studied using a mixed integer linear programming (MILP) approach by Zhang

et al. [16]. An integrated energy systems model that was capable of simultaneously optimizing the design, selection and operation of distributed energy technologies in commercial buildings was showcased by Acha et al. [17]. The performance of various conversion devices portfolios was compared by means of primary energy consumption by Noussan et al. [18]. A two-stage stochastic programming model for the optimal design of distributed energy systems was presented by Zhou et al. [19], without considering electricity, heat and gas network energy flows. An optimal coordinated energy dispatch method for a multi-energy microgrid was proposed by Li and Xu [20], considering a comprehensive set of components. Various flexible conversion and storage devices to maximize flexibility in communities was presented by Good and Mancarella [21]. A multi-energy microgrid sizing model of conversion devices and PV-battery systems using mixed integer linear programming in DER-CAM tool [22], without the detailed energy network studies for operational perspective. Unfortunately, most studies failed to model the thermal energy flows explicitly, and only energy balance constraints were included [23]. There were a few studies that include the electrical power flow and heat transfer equations, and hence the physical and operational constraints of electrical and heating/cooling networks can be modelled [24,25]. Morvaj et al. presented an integrated optimization that incorporates the optimal design and operation of distributed energy systems combined with electrical grid constraints and the design of district heating networks, but without considering battery energy storage [24]. Overall, in most of optimization models and tools, either the set of components was not comprehensive and without a systematic formulation or the detailed network analysis was not conducted by taking into account detailed multi-energy network topologies and locations of energy conversion technologies to calculate network operational variables and losses.

In previous models and tools, detailed network analysis was not conducted by taking into account detailed multi-energy network topologies and locations of generators and energy conversion technologies to calculate network operational variables and losses. In Geidl and Andersson’s energy hub model [26], heating networks were not considered and all the thermal demands are assumed to be met locally at each hub [27]. In the authors’ combined analysis model [2,3], electricity, heat and gas networks were modelled in an integrated manner and with a suitable level of detail for operational purposes. The classical power flow algorithm was extended to use for electrical networks to the multi-energy case, by making use of a whole-system matrix approach that can map conversion devices to locations across different energy networks, suitable for automatic implementations. The results of heat network analysis were validated using SINCAL software and the results

of electrical network analysis were validated using IPISA software [28]. Aiming at the interdependency between energy storage and conversion devices, this paper built an optimal coordinated operation model of storage and conversion devices in multi-energy systems. The core electrical-hydraulic-thermal model [2,3] and the code were consistently used in this paper, which served as a validation of the proposed optimization model. A real case study of a multi-vector district energy system at the University of Manchester was conducted to illustrate the capability of the operation tool. The model comprised two parts:

1. A whole-system optimal operation model was developed for energy conversion devices in multi-vector energy systems, taken into account multi-vector network interactions. By using whole-system matrices, the coupled electrical power, heat power and gas flow equations linked by various energy conversion devices were modelled as an integrated whole. These integrated electrical-hydraulic-thermal-gas flow equations imposed by multi-energy networks was formulated as equality constraints in the optimization. The case study quantified the impact of carbon footprints of grid electricity, energy prices and carbon prices on the operation of energy conversion devices.
2. The design and operation of PV-battery systems was investigated to provide economic incentives for storage owners by taking into account the impact of the integration of conversion devices on the consumer load profiles. The annualized capital expenditure (CAPEX) and annual operating expenditure (OPEX), the self-consumption ratio (SCR), internal return rate (IRR) of PV-battery systems were calculated. The optimization model calculated for each time step the optimal power flows between the PV system, the battery, the grid and the load.

Accordingly, the main contribution of this paper was to fill the gap that the automatic integration of many different kinds of conversion devices and the detailed multi-network operational analysis was not conducted simultaneously in the current optimization. In this paper, electricity, heat and gas networks were modelled in an integrated manner and with a suitable level of detail for operational purposes, by making use of a whole-system matrix approach that can map conversion devices to locations across different energy networks, suitable for automatic implementations. The optimization problem including a significant number of devices and network operational constraints, was formatted as a complex mixed-integer nonlinear programming (MINLP) problem. The proposed sequential method solved the problem by decomposing the multi-energy system into a subsystem of conversion

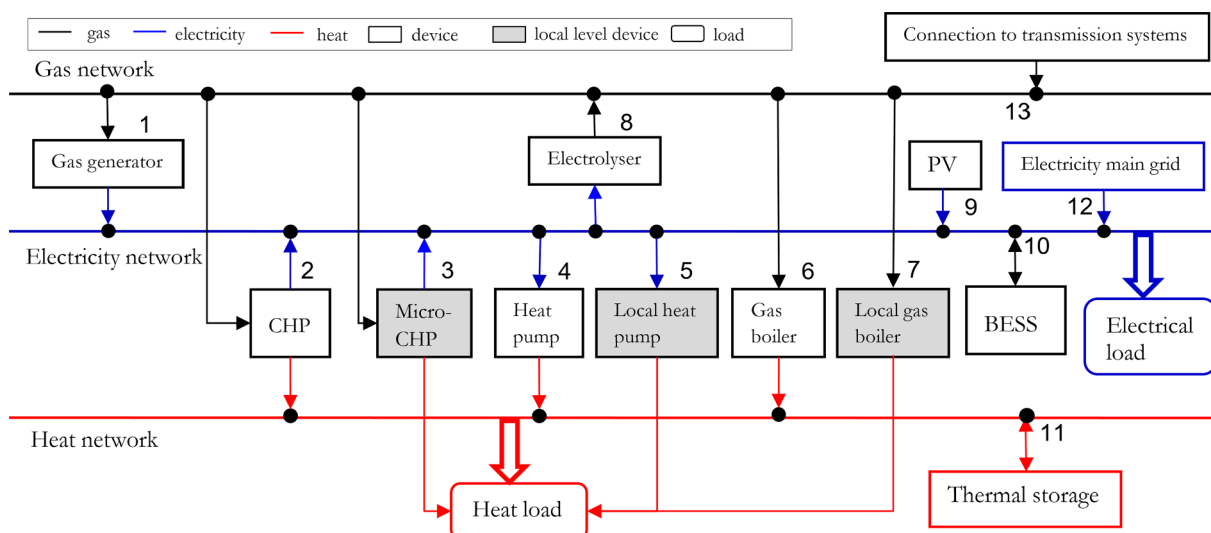


Fig. 1. Schematic of electrical, heat and gas networks with high density of conversion and storage devices.

devices and a subsystem of renewables and storage, which significantly reduced the computation complexity.

## 2. Whole-system modelling of multi-energy networks

A schematic of electrical, heat and gas networks with high density of storage and conversion devices is shown in Fig. 1. By using analogues of power flow analysis, multi-energy flow analysis of natural gas and heat networks were formulated. The independent electrical network model, heat network model (hydraulic and thermal model), gas network model and the model of conversion devices such as turbine generators, CHP, gas boilers and heat pumps were described in the authors' previous papers [2,3]. A variety of energy conversion devices were systematically modelled using a unified matrix approach, to achieve a whole-system matrix analysis of multi-vector systems.

A template for handling input and output data needed for the optimization has been developed in an Excel spreadsheet interface, which is available in the link [29]. More specifically, the Tabs used for input data in the spreadsheet are shown in Appendix A.

The main outputs provided by the optimization model are:

- hourly electrical and heat power (MW) output profiles of the installed technologies;
- battery size (MWh) and its subsequent operation strategy;
- electric power (MW) exchanged between the microgrid and the main grid in time series;
- OPEX comprises fuel cost, carbon cost and operation and maintenance (O&M) cost;
- voltages, active and reactive power, and losses in the electrical network;
- mass flow rates, supply and return temperatures, heat power, and losses in the heat network;
- gas flow rates, nodal pressures, and losses in the gas network.

### 2.1. Integrated electrical-hydraulic-thermal-gas equality constraints

Based on the integrated multi-vector energy flow analysis [2,3], the optimization problem for optimal operation was formulated. In the power flow, only the electrical power at the slack node is unknown. In the optimal energy flow, the heat and electrical power generated from all sources were unknown, as shown in Fig. 2.

Conversion devices allow flows of energy between multi-energy networks. The electrical power generated from the conversion devices at each node are functions of another network. No single network can be analyzed without taking into account the other network. The combined active and reactive power (electricity), hydraulic and thermal (heat), and hydraulic (gas) equations for electrical, heat and gas

networks are expressed as [3]

$$\Delta F(x) = 0 \Rightarrow \begin{cases} P_i - V_i \sum_{j=1}^{N_e} V_j (G_{ij} \cos \theta_{ij} + B_{ij} \sin \theta_{ij}) \leftarrow \text{Active power} \\ = 0 \\ Q_i - V_i \sum_{j=1}^{N_e} V_j (G_{ij} \sin \theta_{ij} - B_{ij} \cos \theta_{ij}) \leftarrow \text{Reactive power} \\ = 0 \\ C_p A_h \dot{m} (T_s - T_o) - \Phi = 0 \leftarrow \text{Heat power} \\ B_h K_h \dot{m} |\dot{m}| = 0 \leftarrow \text{Loop pressure - heat} \\ C_s T_s - b_s = 0 \leftarrow \text{Supply temperature} \\ C_r T_r - b_r = 0 \leftarrow \text{Return temperature} \\ A_g v_g - v_q = 0 \leftarrow \text{Gas flow} \\ B_g K_g v_g |v_g^{k-1}| = 0 \leftarrow \text{Loop pressure - heat} \end{cases} \quad (1)$$

where  $P$  is active power (MW),  $Q$  is reactive power (MVar).  $V$  is the voltage magnitude (p.u.),  $\theta$  is the voltage angle (rad).  $N_e$  is the number of busbars in the electricity network;  $Y_{ij} = G_{ij} + jB_{ij}$  is the admittance that relates current injection at a busbar to the busbar voltage,  $i$  and  $j$  are busbar numbers. The electrical network incidence matrix  $A_e$  is used to form the admittance matrix  $Y$  [30,31].  $A$  is the network incidence matrix that relates the nodes to the branches. The subscript  $e$  represents electricity network.

For heat flows,  $C_p$  is the specific heat of water ( $J \text{ kg}^{-1} \text{ }^\circ\text{C}^{-1}$ ),  $C_p = 4.182 \times 10^{-3} \text{ MJ kg}^{-1} \text{ }^\circ\text{C}^{-1}$ .  $\dot{m}$  is the vector of the mass flow ( $\text{kg/s}$ ) within each pipe. The subscript  $h$  represents heat network.  $\Phi$  is the vector of heat power (MW) consumed or supplied at each node.  $T_s$  is the supply temperature;  $T_o$  is the outlet temperature (temperature at the outlet of each node before mixing in the return network) and  $T_r$  is the return temperature. The subscript  $s$  represents supply network and the subscript  $r$  represents return network.  $B$  is the loop incidence matrix that relates the loops to the branches.  $K$  is the vector of the resistance coefficients of each pipe.  $C$  is a matrix of coefficients and  $b$  is a column vector of solutions formed in the thermal model (details were described in [28]).

For gas flows,  $v_g$  is the vector of the gas flow rate within each pipe ( $\text{m}^3/\text{h}$ ), and the subscript  $g$  represents gas network.  $v_q$  is the vector of the gas flow through each node injected from a source or discharged to a load, and the subscript  $q$  represents nodal variables.

### 2.2. Efficiency matrix

The efficiency of a piece of infrastructure is a measure of the energy input versus the energy output. From the input data, multi-network incidence matrices that relate the numbering of conversion device nodes to corresponding network nodes and one whole-system multi-energy

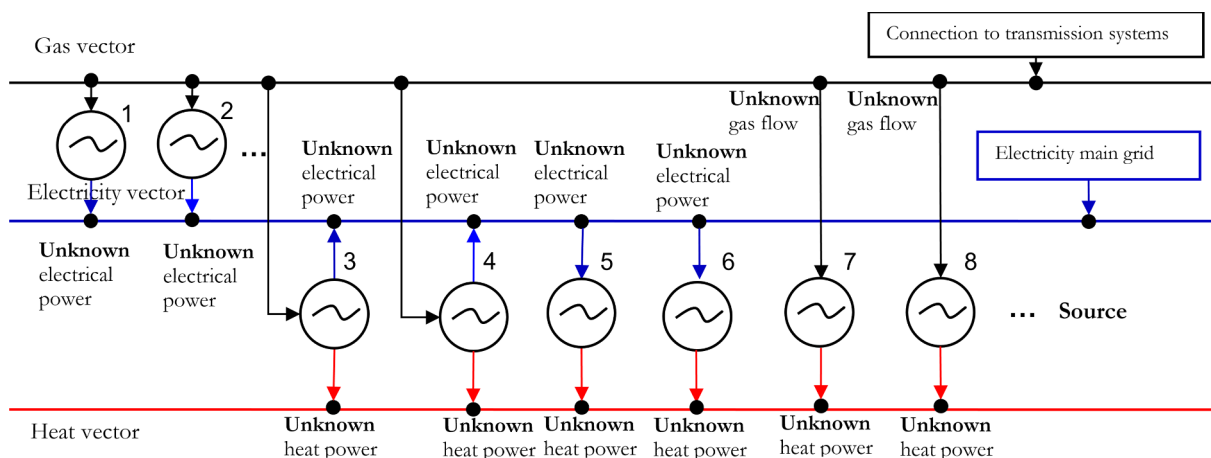


Fig. 2. Unknown input of conversion devices in optimal operation.

conversion efficiency matrix are generated automatically [3].

Schematic of the relation between conversion devices and multi-energy networks is shown in Fig. 3. Based on various energy vectors that the conversion device nodes are linked, conversion devices at nodes numbering 1, 2, 3 and 4 could be gas generator, CHP, heat pump and gas boiler respectively. In the multi-energy efficiency matrix  $\mathcal{H}$ , there are as many columns as transformations, for example, three columns in the case of gas to electricity, gas to heat, electricity to heat. There are as many rows as the number of conversion devices in the district. Each element of the matrix is the relevant conversion efficiency from one energy vector to another energy vector.

### 2.3. Permutation matrices

A numbering approach using permutation matrix operation has been used to model the topology of different networks and their linkages through conversion devices. Permutation matrix is formed from the node numbering of conversion devices in input data. Following Fig. 3, the numbering of conversion devices mapping to their corresponding multi-vector energy networks is shown in Table 1.

For instance, (1 4) represents a conversion device numbering 1 is mapped to local numbering 4 in its electrical network. The permutation of the numbering of conversion devices to the electrical network is expressed as

$$\alpha_e = (1\ 4)(2\ 5)(3\ 3) \quad (2)$$

A permutation matrix is a matrix obtained by permuting the rows of an  $n \times n$  identity matrix according to some permutation of the numbers 1 to  $n$ . Every row and column therefore contains precisely a single 1 with 0s everywhere else, and every permutation corresponds to a unique permutation matrix [32].

The permutation matrix  $M_e$  for the electricity vector is then formed accordingly. There are as many columns as electricity busbars. Elements shown in Eq. (2) are put as 1 in the permutation matrix  $M_e$ , while all the other elements are put as zero. Thus, the electricity permutation matrix mapping conversion devices to the electrical network is formed as

$$M_e = \begin{bmatrix} 0 & 0 & 0 & 1 & 0 \\ 0 & 0 & 0 & 0 & 1 \\ 0 & 0 & 1 & 0 & 0 \\ 0 & 0 & 0 & 0 & 0 \end{bmatrix} \quad (3)$$

The permutation matrices for heat and gas vectors are then formed similarly. Through this, the electrical power, heat power and gas flow of each conversion device is mapped to its located multi-vector energy network. The electrical power in the electricity network for this example is expressed as

$$P_{con}^{local} = \begin{bmatrix} P_{e1} \\ P_{e2} \\ P_{e3} \\ P_{e4} \\ P_{e5} \end{bmatrix} = (M_e)^T P_{con}^{global} = \begin{bmatrix} 0 & 0 & 0 & 0 \\ 0 & 0 & 0 & 0 \\ 0 & 0 & 1 & 0 \\ 1 & 0 & 0 & 0 \\ 0 & 1 & 0 & 0 \end{bmatrix} \begin{bmatrix} P_1 \\ P_2 \\ P_3 \\ P_4 \end{bmatrix} = \begin{bmatrix} 0 \\ 0 \\ P_3 \\ P_1 \\ P_2 \end{bmatrix} \quad (4)$$

### 2.4. Mapping of conversion devices to multi-energy networks

By using the multi-energy efficiency matrix  $\mathcal{H}$  and the permutation matrix  $M$ , the models of conversion devices are automatically incorporated in the terms  $P$ ,  $\Phi$ ,  $v_q$  of the multi-vector flow equation (1). Let us denote the matrix of end-use demand (e.g., electrical power and heat power) at the conversion devices as  $E^{out}$ . The matrix of input electrical power and gas flows at the conversion devices is denoted as  $E^{in}$ . The matrices  $\mathcal{H}$ ,  $E^{in}$  and  $E^{out}$  have the same dimension, e.g.,  $N_{con} \times 3$ , where  $N_{con}$  is the number of total conversion devices. The elements  $E_{ij}^{in}$  are equal to the elements  $E_{ij}^{out}$  divided by the

corresponding element of the conversion efficiency matrix  $\mathcal{H}_{ij}$ .

$$E_{ij}^{in} = E_{ij}^{out} / \mathcal{H}_{ij} \quad (5)$$

where  $i$  is the node numbering of conversion devices,  $j$  is the column index. In the example of Fig. 3 and Table 1, for  $\mathcal{H}$ , the columns comprise  $ge$ ,  $gh$ ,  $eh$  (gas to electricity, gas to heat, electricity to heat, respectively). For  $E^{in}$ , the columns comprise *gas*, *gas*, *electricity*. For  $E^{out}$ , the columns comprise *electricity*, *heat*, *heat*. For example, the electrical power from a conversion device  $P_{con,i}$  is determined by  $\Phi_{con,i}$ .

$$P_{con,i} = \Phi_{con,i} / \mathcal{H}_{con,i,e \rightarrow h} \quad (6)$$

where  $\mathcal{H}_{con,i,e \rightarrow h}$  is the electricity-to-heat efficiency of a conversion device such as a heat pump.

A flowchart describing the integration of conversion device models into the multi-vector network equations is shown in Fig. 4 [3]. Conversion devices at nodes that coupled multiple energy networks were described using efficiency matrix. The input and output vectors of conversion devices were then mapped to corresponding network equations using permutation matrices.

### 2.5. Energy flows of PV-battery systems

The optimization model is indexed by the sets  $(d, t)$ , where  $d$  is the set of days in a year ( $1 \leq d \leq 365$ ) and  $t$  is the set representing the hour periods in each day ( $1 \leq h \leq 24$ ). As the power from the PV system can be consumed directly or via the battery energy storage systems (BESS) or fed into the grid, the different power flows have to satisfy the following constraint as well.

$$P_{PV \rightarrow load}(d, t) + P_{PV \rightarrow BESS}(d, t) + P_{PV \rightarrow grid}(d, t) = P_{PV}(d, t) \quad (7)$$

where  $P_{PV}(d, t)$  is the electric power generated from PV (kW).  $P_{PV \rightarrow load}(d, t)$  is the electric power supplied to the load from PV (kW).  $P_{PV \rightarrow BESS}(d, t)$  is the electric power charging to the battery from PV (kW).  $P_{PV \rightarrow grid}(d, t)$  is the electric power exported to the grid from PV (kW).

The load balance equation ensures that the load can be satisfied by the PV, by the battery or by the grid.

$$P_{BESS}^{discharge}(d, t) - P_{BESS}^{charge}(d, t) + P_{PV}(d, t) + P_{grid}(d, t) = P_{load}(d, t) \quad (8)$$

where  $P_{BESS}^{charge}$  is charging rate (kW) – the maximum rate at which the battery device consumed electricity when recharging.  $P_{BESS}^{discharge}$  is discharging rate (kW) – the maximum rate at which the battery device generated electricity when discharging.

Substituting Eq. (7) into Eq. (8),

$$P_{BESS}^{discharge} - P_{BESS}^{charge} + P_{PV \rightarrow load} + P_{PV \rightarrow BESS} + P_{PV \rightarrow grid} + P_{grid} = P_{load} \quad (9)$$

Energy flows of PV to the load, the battery and the grid depend on the value of PV generation and the load as shown in Fig. 5. The priority of energy flows from PV is: 1. PV  $\rightarrow$  load, 2. PV  $\rightarrow$  BESS, 3. PV  $\rightarrow$  grid.

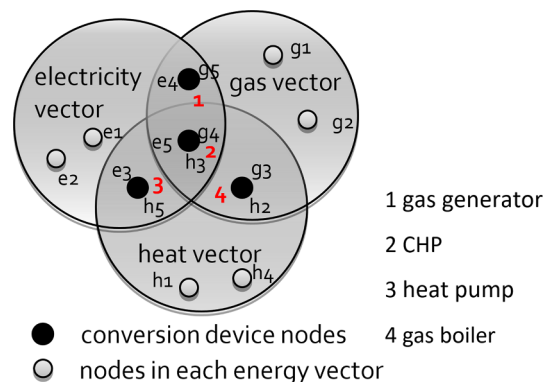
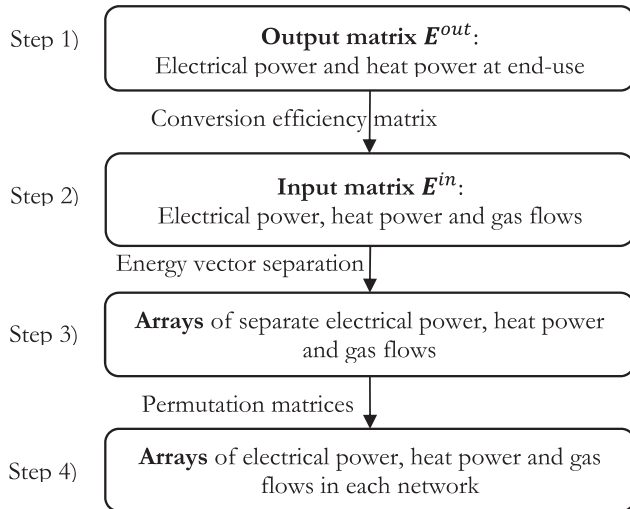


Fig. 3. Schematic of numberings of conversion devices.

**Table 1**  
Numbering of conversion devices mapping to the corresponding multi-networks.

Conversion device No.	No. in electrical network	No. in heat network	No. in gas network
1	e4	–	g5
2	e5	h3	g4
3	e3	h5	–
4	–	h2	g3



**Fig. 4.** Flowchart of the integration of conversion device models into the multi-vector network equations.

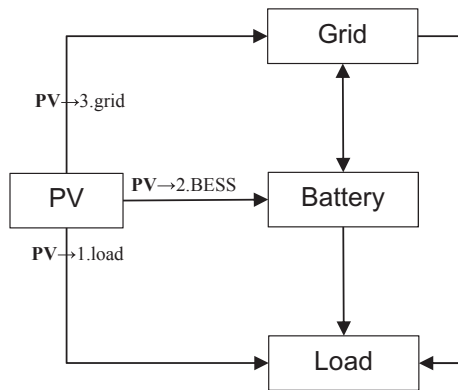


**Fig. 5.** Schematic of energy flows of PV to the load, the battery and the grid.

When the PV electricity is surplus for the load, the program optimises the proportion of PV electricity charged to the battery and exported to the grid.

Three parts of energy flows from PV generation to the load are expressed using decision variables  $P_{BESS}^{charge}$  or  $P_{BESS}^{discharge}$  as shown in Table 2, and details are discussed as follows

- If the generated power of PV is smaller than the load, then PV

electricity is all supplied to the load.

- If the generated power of PV is larger than the load and the surplus does not exceed the battery charging limit, then the PV to BESS charging rate  $P_{PV \rightarrow BESS}$  is equal to the surplus  $P_{PV} - P_{load}$ . Otherwise,  $P_{PV \rightarrow BESS}$  is equal to the battery maximum charging power  $P_{BESS}^{charge}$ . Hence,  $P_{PV \rightarrow BESS}$  is expressed as  $\min\{P_{PV} - P_{PV \rightarrow load}, P_{BESS}^{charge}\}$ , since the expression  $P_{PV \rightarrow BESS} = P_{PV} - P_{load}$  does not include the case that the surplus PV may exceed the battery charging limit at that period and the expression  $P_{PV \rightarrow BESS} = P_{BESS}^{charge}$  does not include the case that a proportion of the battery charging power may come from the grid electricity.
- If there is surplus PV electricity after charging to BESS, then the exported power from PV  $P_{PV \rightarrow grid}$  is equal to net PV generated power  $P_{PV} - P_{load}$  subtracting  $P_{PV \rightarrow BESS}$ . Otherwise,  $P_{PV \rightarrow grid}$  is equal to zero.

The arbitrage of the battery was gained from the difference between grid electricity price when storing electricity and discharging electricity. For PV-battery systems, the surplus PV electricity was charged to the battery and then discharged in the evening peak price period. The extra benefit of the PV-battery coupling ( $P_{PV \rightarrow BESS}$ ) was gained from the difference between the cheap PV FiT export tariff and the grid electricity price of discharging the stored surplus PV electricity.

### 2.6. Self-consumption definition and metrics

The economic incentive to install a solar PV system depends increasingly on using PV generation on-site (‘self-consumption’) rather than receiving payments from generating electricity and exporting it to the grid. There is, however, remarkably little empirical evidence on self-consumption [9]. A battery offers the opportunity to match the PV energy supply with the respective load profile and thus significantly increase the self-consumption ratio (SCR) and the self-sufficiency ratio (SSR) [33].

The share of self-consumption is defined as the ratio of energy which is generated by the PV system and directly used at the installation site ( $E_{PV,used}$ ) to the total amount of energy generated ( $E_{PV,gen}$ ).

$$SCR = \frac{\text{self-consumed PV electricity}}{\text{total electricity generation from PV}} = \frac{E_{PV,used}}{E_{PV,gen}} = \frac{\sum P_{PV \rightarrow load} + \sum P_{PV \rightarrow BESS}}{\sum P_{PV}} \quad (10)$$

The degree of self-sufficiency is defined as the ratio of energy which is generated by the PV system and directly used at the installation site ( $E_{PV,used}$ ) to the total amount of energy used by the household. The SSR describes energy independency of the PV-battery systems in the community.

$$SSR = \frac{\text{self-consumed PV electricity}}{\text{total electricity demand}} = \frac{E_{PV,used}}{E_{load}} = \frac{\sum P_{PV \rightarrow load} + \sum P_{PV \rightarrow BESS}}{\sum P_{load}} \quad (11)$$

The ratio of battery capacity to PV power determines the increase in self-consumption. By increasing the self-consumption quota, the electricity generated from the PV-battery system may compete with the costs for electricity from the grid.

**Table 2**  
Energy flows of a PV-battery system with relation to PV generated power and the load.

Conditions	$P_{PV \rightarrow load}$	$P_{PV \rightarrow BESS}$	$P_{PV \rightarrow grid}$
$P_{PV} > P_{load}$	$P_{load}$	$\min\{P_{PV} - P_{PV \rightarrow load}, P_{BESS}^{charge}\}$	$P_{PV} - P_{PV \rightarrow load} - P_{PV \rightarrow BESS}$
$P_{PV} \leq P_{load}$	$P_{PV}$	0	0

### 3. Whole-system optimal coordinated operation

#### 3.1. Framework of optimization

As an extension to the combined analysis of multi-energy flows, a whole-system optimization method of multi-vector energy systems was developed. The optimal operation of energy conversion devices in multi-vector energy systems is modelled, taken into account multi-vector network interactions. In the formulation of optimal operation, the integrated electrical-hydraulic-thermal-gas equations was included as equality constraints. An overview of generic optimization model of a multi-vector energy system is shown as Fig. 6, consisting of inputs describing the system, constraints defining the behavior of the system and the output which gives the performance of the system [24].

#### 3.2. Interdependency between energy storage and conversion devices

The term net load refers to the system demand minus the local generation from variable resources. For off-grid solar PV systems, the net load uncertainty is the main factor that controls its operation and planning. Therefore, the need for energy storage is essential to mitigate this uncertainty. The optimization aims at quantifying BESS capacity required and the operation strategy to effectively manage net load fluctuations.

On one hand, the inevitable penetration of variable generation and electrification of heat and transport leads to increasingly variable operation of thermal dispatchable generators. On the other hand, the integration of heating and cooling devices (e.g. CHP, gas boilers, heat pumps, air conditioners, absorption chillers) is expected to have a major impact on consumer load profiles. In this paper, the optimal operation of energy storage and conversion devices considering interdependency in multi-vector energy systems was studied as shown in Fig. 7. Specifically, the impact of increasing net-load variability on the design and operation of cost optimized PV-battery systems was assessed.

The coordination is operated by an Aggregator, run by the two subsystems comprising conversion devices and PV-battery systems. The Aggregator is a technical and commercial intermediary enabler that allows conversion devices and PV-battery systems to communicate. The Aggregator schedules the conversion devices and energy storage systems to maximize the income received without exceeding the multi-energy network operational limits. This is achieved by requesting the BESS to change the charging/discharging schedule to maximize

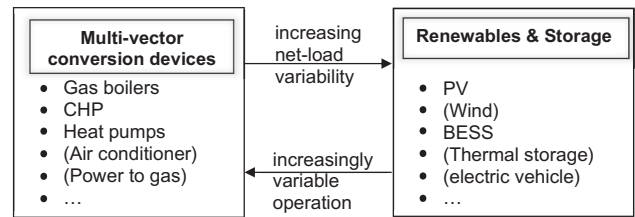


Fig. 7. Interdependency and coordination between renewables, energy storage and conversion devices.

arbitrage revenue based on the optimal output of conversion devices. Additional income is obtained for the additional electricity self-consumption in coordination. The additional income obtained is allocated so that both subsystems have an economic incentive to be operated in a coordinated manner [34].

The system devices are scheduled in “last-in, first-off” operation and the BESS is connected last. The operation of the Aggregator is described as follows [34]:

1. The Aggregator receives from conversion devices their anticipated outputs and the anticipated charge/discharge schedule from the BESS. Conversion devices make their projections based on heat and power load forecasts. Energy storage systems make their projections considering the electricity time-of-use (TOU) tariff and the prediction of PV generation.
2. The Aggregator assesses whether the multi-energy network operational rating is exceeded by the anticipated outputs. If the limit is not exceeded, the Aggregator accepts the anticipated outputs and takes no further action. If the limit is exceeded, the Aggregator runs an optimization algorithm to schedule conversion devices and the energy storage systems, as described in Step 3.
3. The optimization algorithm has an objective function (Eqs. (12) and (13)) to minimize the total cost to meet electricity and heat demand. Eq. (12) is relative to the income of conversion devices and Eq. (13) refers to the income of the energy storage systems.

#### 3.3. Sequential method

The optimization can be decomposed into sequential modelling of conversion devices and PV-battery systems. Sequential method was proposed in the authors’ previous work [2] and was also used in Ref. [35]. In the sequential mode as shown in Fig. 8, only one iteration

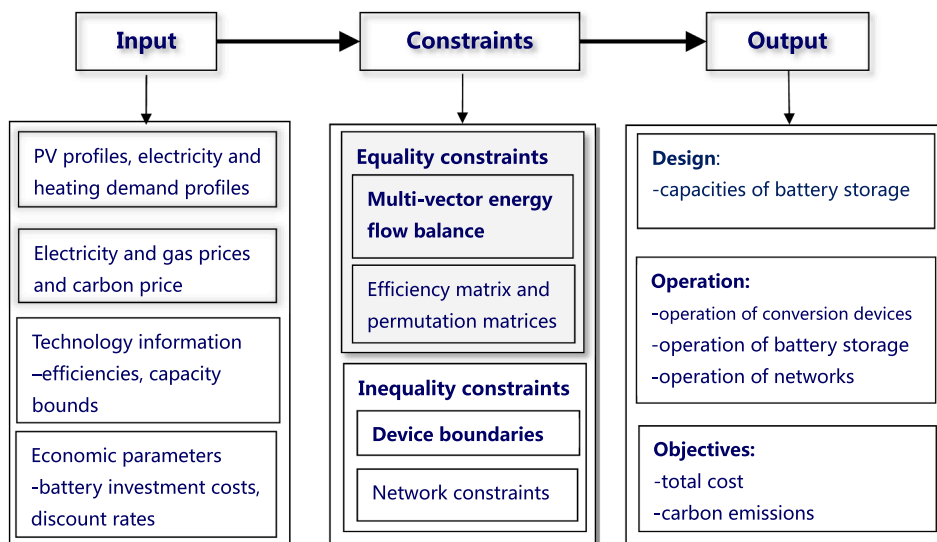


Fig. 6. Overview of the optimization of multi-vector energy systems.

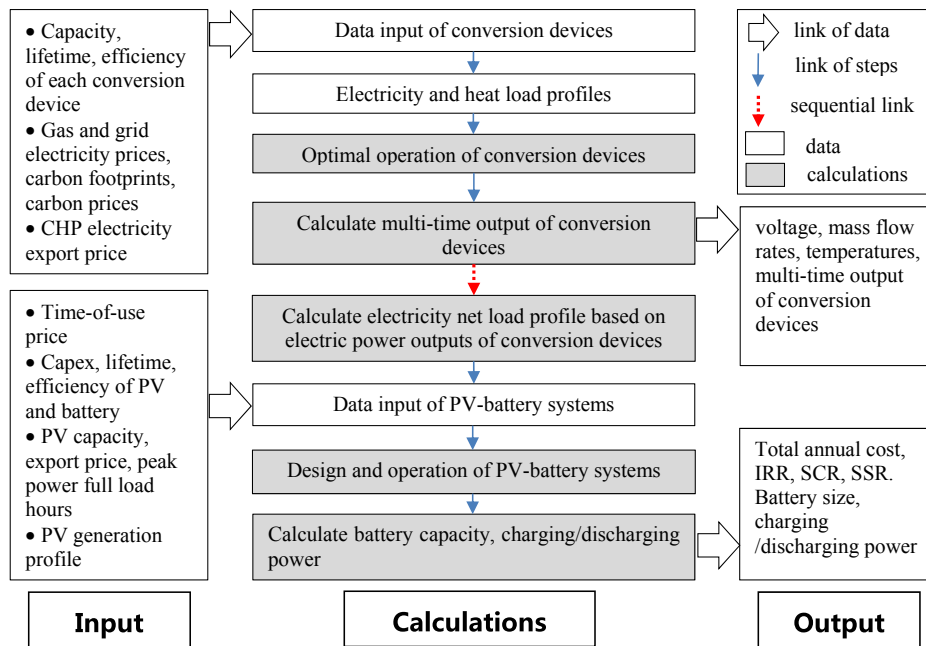


Fig. 8. Flowchart of sequential method of optimal operation of conversion devices and PV-battery systems.

between conversion devices and PV battery systems was used when the operation of conversion devices is inflexible such as without thermal storage. The framework does not include all these considerations in a single mathematical model, as this may be computationally challenging or infeasible [25]. The operation of conversion devices (including economic dispatch and power flow) was optimized to minimize the total operating expenditure (including fuel cost, carbon cost and maintenance cost) and the optimal electric power generation or consumption was obtained. In this approach, the electric power generation or consumption of conversion devices was provided as an input to the optimization of PV-battery system model. In this modelling, the total annualized cost of conversion devices was minimized and afterwards the total annualized cost of PV-battery systems was minimized. The red (dashed) line indicates the sequential link of conversion devices and PV-battery systems. The sequential approach does not consider the PV-battery systems constraints while optimising the conversion devices systems. Hence, a disadvantage of this modelling is that the PV-battery operation does not influence the operation of conversion devices, as the modelling of conversion devices is carried out before the PV-battery systems modelling. Furthermore, the sequential method is limited to multi-energy systems that purchase a significant fraction of their electricity from the electricity grid. For example, if a system had a large power plant capable of producing electricity at a lower price than the grid, then it would fulfill the entire electricity requirements before the PV-battery step is reached, and thus the PV system would never be used.

### 3.4. Objective function

Multi-objective programming represents a very useful generalization of mono objective approaches, which helps to incorporate the different stakeholder points of view that need to be considered. In addition to the first objective related to the total operating expenditure (OPEX), the second objective related to carbon emissions was considered in the objective function. The impact of whether or not considering carbon prices on conversion devices was investigated. Similarly, other objective function such as voltage deviation, loss and reliability could be readily applied too and consistently with the optimal operation model proposed. The presented work could be considered as a simple form of multi-objective function using weight

method, while a full set of Pareto optimal solutions would need to be run to address the more complicated multi-objective optimization in future work. In Pareto optimal solutions, no improvement is possible in any objective without sacrificing at least one of the other objective functions. The so-called Pareto frontier, represents the set of optimal points that can be considered to be optimal in terms of one or both of the two objectives [36].

#### 3.4.1. Conversion devices

The objective function is to minimize the operating expenditure (OPEX) of conversion devices, which includes the cost of fuel consumed, the cost of carbon and the operating and maintenance costs of the components (O&M cost). The fuel cost is calculated as the cost of electricity and gas purchased from the network minus the revenue from electricity sold to the grid [37–39].

$$C_{OpeX-DER} = C_e P_{import} + C_g v_{gtotal} + C_{carbon} \xi_e P_{import} + C_{carbon} \xi_g v_{gtotal} + C_{O\&M} \tag{12}$$

fuelcost carboncost

where  $C_e$ —electricity spot price (£/MWh),  $P_{import}$ —imported electric power (MW),  $C_g$ —natural gas price (£/MWh),  $v_{gtotal}$ —total consumed natural gas flow rate (m<sup>3</sup>/h),  $\xi_e$ —electricity carbon footprints (gCO<sub>2</sub>/kWh),  $\xi_g$ —gas carbon footprints (gCO<sub>2</sub>/kWh),  $C_{carbon}$ —carbon price (£/tonne).  $C_{O\&M}$ —O&M costs including fixed share of O&M and the variable O&M costs; fuel costs are not included.

#### 3.4.2. PV-battery systems

The objective function is to minimize the overall cost of PV-battery systems, which consists of annuitized investment cost associated with storage assets and the annual operating cost shown as Eq. (13), which includes:

- annualized capital expenditure (CAPEX) of PV-battery systems;
- annual operating expenditure (OPEX).

$$Min C_{total\_PVB} = LF_n \cdot C_{Capex\_BESS} + C_{OpeX\_PVB} \tag{13}$$

where  $C_{total\_PVB}$ —lifetime annualized cost of PV-battery systems,  $C_{OPEX\_PVB}$ —annual OPEX of PV-battery systems including O&M and fuel costs,  $C_{CAPEX\_BESS}$ —up-front CAPEX cost of BESS.  $LF_n$ —the levelised factor over  $n$  years,  $LF_n = \frac{d(1+d)^n}{(1+d)^n - 1}$  [37], where  $d$  is the discount rate,  $n$

is devices' lifetime (years).

The CAPEX of BESS is expressed as

$$C_{\text{Capex-BESS}} = C_{\text{BESS}}^E E_{\text{BESS}}^{\text{rated}} + C_{\text{BESS}}^P P_{\text{BESS}}^{\text{rated}} \quad (14)$$

where  $C_{\text{BESS}}^E$  denotes the energy-capacity-determined cost for a battery and  $E_{\text{BESS}}^{\text{rated}}$  is the rated storage capacity of the battery.  $C_{\text{BESS}}^P$  denotes the power-capacity-determined cost for a battery and  $P_{\text{BESS}}^{\text{rated}}$  is the rated power of the battery inverter. The capacity itself is calculated as the power rating multiplied by the number of hours that it is assumed to operate at full power.  $C_{\text{PV}}^{\text{capex}}$  is the capital cost of a PV panel per kW and  $P_{\text{PV}}^{\text{rated}}$  is the rated peak power of the PV system. A certain percentage of planning capacity reserve margin (typically 5–15%) is considered above the demand requirements to account for unexpected system events [40].

The annual revenue comprises the arbitrage revenue from the battery and the revenue of the electricity replaced by the PV, electricity exported to the main grid and the PV subsidy. The energy arbitrage from the battery is achieved by: 1. shifting electricity consuming from lower price to higher price; 2. using cheap surplus electricity generated from PV that would otherwise be exported to the grid.

The OPEX equals the cost of grid electricity consumed  $P_{\text{grid}}$ , which is expressed as

$$C_{\text{Opex-PVB}} = \sum_{(d,t)} P_{\text{grid}}(d, t) C_e(t) \quad (15)$$

Following Eq. (9) and taking  $P_{\text{grid}}$  at the left side,

$$P_{\text{grid}} = (P_{\text{load}} - P_{\text{PV} \rightarrow \text{load}}) + (P_{\text{BESS}}^{\text{charge}} - P_{\text{BESS}}^{\text{discharge}} - P_{\text{PV} \rightarrow \text{BESS}}) - P_{\text{PV} \rightarrow \text{grid}} \quad (16)$$

Hence, the OPEX of the PV-battery system is written as Eq. (17). The electricity consumed by the original load  $P_{\text{load}}$  is constant and is thus not considered. The cost is divided into three parts: 1. load consumption which is reduced by the PV self-consumption; 2. energy charge and discharge from the battery which is reduced by using cheap surplus electricity generated from PV; 3. cost reduction of the PV electricity export to the grid and the subsidy of the PV installation.

$$C_{\text{Opex-PVB}} = \sum_{(d,t)} (P_{\text{load}} - P_{\text{PV} \rightarrow \text{load}}) C_e(t) + (P_{\text{BESS}}^{\text{charge}} - P_{\text{BESS}}^{\text{discharge}} - P_{\text{PV} \rightarrow \text{BESS}}) C_e(t) - C_{\text{PV}}^{\text{export}} \sum_{(d,t)} P_{\text{PV} \rightarrow \text{grid}} - C_{\text{PV}}^{\text{subsidy}} \sum_{(d,t)} P_{\text{PV}} \quad (17)$$

where  $C_{\text{PV}}^{\text{export}}$  is the PV export feed-in tariff (£/kWh).  $C_{\text{PV}}^{\text{subsidy}}$  is the subsidy price of electricity generated from PV (£/kWh). Following Table 2, when  $P_{\text{PV}} > P_{\text{load}}$ ,  $P_{\text{PV} \rightarrow \text{load}} = P_{\text{load}}$ ,  $P_{\text{PV} \rightarrow \text{BESS}} = \min\{P_{\text{PV}} - P_{\text{PV} \rightarrow \text{load}}, P_{\text{BESS}}^{\text{charge}}\}$ ,  $P_{\text{PV} \rightarrow \text{grid}} = P_{\text{PV}} - P_{\text{PV} \rightarrow \text{load}} - P_{\text{PV} \rightarrow \text{BESS}}$ ; when  $P_{\text{PV}} \leq P_{\text{load}}$ ,  $P_{\text{PV} \rightarrow \text{load}} = P_{\text{PV}}$ ,  $P_{\text{PV} \rightarrow \text{BESS}} = 0$ ,  $P_{\text{PV} \rightarrow \text{grid}} = 0$ .

### 3.5. Constraints

A binding or an active inequality constraint is an inequality constraint that is satisfied exactly [41]. A few inequality constraints of node temperatures and voltages may be binding or active during the optimization search process.

#### 3.5.1. Conversion devices

##### (1) Equality constraints

By using whole-system matrices, the coupled electrical power, heat power and gas flow equations linked by various energy conversion devices were modelled as an integrated whole. These integrated electrical-hydraulic-thermal-gas flow equations imposed by multi-energy networks was formulated as equality constraints in the optimization.

The equality constraints were formed by multi-vector energy flow balance Eq. (1) based on whole-system matrices modelling. The input and output of conversion devices coupled multi-vector networks were modelled by their efficiency matrix and permutation matrices.

##### (2) Conversion device constraints

Installed capacities of all conversion devices must be between their lower bound and upper bound. The electrical or heat power outputs has to be smaller than or equal to the installed capacity

$$\begin{aligned} P_{\text{con}_i}^{\text{min}} &\leq P_{\text{con}_i} \leq P_{\text{con}_i}^{\text{max}} \\ \varnothing_{\text{con}_i}^{\text{min}} &\leq \varnothing_{\text{con}_i} \leq \varnothing_{\text{con}_i}^{\text{max}} \end{aligned} \quad (18)$$

where  $P_{\text{con}_i}$  and  $\varnothing_{\text{con}_i}$  are the electric power or heat power output of conversion device  $i$ . The subscript  $\text{con}$  represents a conversion device generating electricity or heat.

##### (3) Electricity network constraints

Busbar voltage magnitudes must be kept at acceptable levels. The voltage tolerance of (+10%/−6%) for the LV network is not breached at any busbar. The generated electric power from generators represented by  $P_{\text{gen}_i}$  and  $Q_{\text{gen}_i}$  must be restricted by its lower and upper limits. The power carrying capacity of feeders ( $P_{ij}$ ) through any branch  $ij$  must be well within the maximum thermal capacity of the lines.

$$\begin{aligned} V_i^{\text{min}} &\leq V_i \leq V_i^{\text{max}}, i = 1, \dots, N_e \\ P_{\text{gen}_i}^{\text{min}} &\leq P_{\text{gen}_i} \leq P_{\text{gen}_i}^{\text{max}}, i = 1, \dots, N_{ge} \\ Q_{\text{gen}_i}^{\text{min}} &\leq Q_{\text{gen}_i} \leq Q_{\text{gen}_i}^{\text{max}}, i = 1, \dots, N_{ge} \\ |P_{ij}| &\leq P_{ij}^{\text{max}}, i, j = 1, \dots, N_e \end{aligned} \quad (19)$$

where  $N_e$  is the number of busbars,  $N_{ge}$  is the number of generators.

##### (4) Heat network constraints

Supply and return temperatures at each node were set within limits:

$$\begin{aligned} T_s^{\text{min}} &\leq T_s \leq T_s^{\text{max}} \\ T_r^{\text{min}} &\leq T_r \leq T_r^{\text{max}} \end{aligned} \quad (20)$$

The mass flow rate within each pipe in the heat network was set to be within minimum and maximum limits:

$$\dot{m}_{\text{min}} \leq \dot{m} \leq \dot{m}_{\text{max}} \quad (21)$$

##### (5) Gas network constraints

The gas pressure at each node was set within limits:

$$P_g^{\text{min}} \leq P_g \leq P_g^{\text{max}} \quad (22)$$

The gas flow rate within each pipe was set within limits:

$$v_g^{\text{min}} \leq v_g \leq v_g^{\text{max}} \quad (23)$$

where  $v_g$  is the vector of the gas flow rate within each pipe ( $\text{m}^3/\text{h}$ ).

#### 3.5.2. PV-battery systems

Degradation of the battery is not considered, though it could be considered in future work in this area [4]. The battery constraints are expressed as follows:

i. the charge/discharge rate must be within the battery power rating.

$$\begin{aligned} 0 &\leq P_{\text{BESS}}^{\text{charge}}(d, t) \leq P_{\text{BESS}}^{\text{rated}} \\ 0 &\leq P_{\text{BESS}}^{\text{discharge}}(d, t) \leq P_{\text{BESS}}^{\text{rated}} \end{aligned} \quad (24)$$

In the meantime, the battery discharging rate cannot exceed the

load minus the supply from the PV, plus the electric power limit exported to the grid.

$$P_{BESS}^{discharge}(d, t) \leq \max(P_{load} - P_{PV}, 0) + P_{export}^{limit} \quad (25)$$

where  $P_{export}^{limit}$  is the limit of exported electric power to the main grid.

The charging is organized by setting an upper demand limit on the grid [42]. The charging rate plus the load may not exceed this limit. Following Eq. (8),

$$P_{grid}(d, t) = P_{BESS}^{charge}(d, t) - P_{BESS}^{discharge}(d, t) - P_{PV} + P_{load} \leq P_{import}^{limit} \quad (26)$$

where  $P_{import}^{limit}$  is the limit of imported electric power from the main grid.

The battery cannot be charged and discharged simultaneously, which is expressed as Eq. (27). However, taken into account the charging and discharging efficiency in Eq. (28), this constraint (27) is proved to be redundant. Under normal operating conditions the model has no incentive for simultaneous charging and discharging and therefore constraint will limit either  $P_{BESS}^{charge}$  or  $P_{BESS}^{discharge}$  to the maximum rated power of the battery inverter  $P_{BESS}^{rated}$  [43].

$$P_{BESS}^{charge}(d, t)P_{BESS}^{discharge}(d, t) = 0 \quad (27)$$

ii. stored energy balance constraints [44]

$$E_{BESS}(d, t) = E_{BESS}(d, t - 1) + (\eta_c P_{BESS}^{charge}(d, t) - P_{BESS}^{discharge}(d, t)/\eta_d)\Delta t \quad (28)$$

where  $\eta_c$  is the battery charging efficiency and  $\eta_d$  is the discharging efficiency. If the data resolution is half an hour, then  $\Delta t$  is equal to 1/2.

iii. the storage content at the first time step of the optimization period to the minimum state of charge in percent of the rated capacity [43].

$$E_{BESS}(d, 0) = E_{BESS}(d, t_{end}) = SOC_{min} E_{BESS}^{rated} \quad (29)$$

where SOC represents the State of Charge of the battery.  $t_{end}$  is the last time step in the battery daily operation.

iv. constraints associated with the amount of energy that can be stored

$$SOC_{min} E_{BESS}^{rated} \leq E_{BESS}(d, t) \leq SOC_{max} E_{BESS}^{rated} \quad (30)$$

### 3.6. Solutions

The variables are the unknowns in the optimization model. The vector of variables for conversion devices is

$$\mathbf{x} = [\theta \quad |V| \quad P_{con} \quad \dot{m} \quad T_s \quad T_r \quad \varnothing_{con} \quad \mathbf{v}_g]^T \quad (31)$$

where  $P_{con}$  and  $\varnothing_{con}$  are the outputs (electric power and heat power) of conversion devices. The subscript *con* represents a conversion device generating electricity or heat.

Assuming the resolution is  $t_{int}$  hour, then the total snapshots in a day  $N_t$  is equal to  $24/t_{int}$ . The decision variables of the PV-battery system optimization model are visualized as shown in Fig. 9. In the figure,  $x$  denotes variables in power (kW) and  $y$  denotes variables in energy (kWh). SOC represents the State of Charge of the battery.

The proposed sequential method was used to solve the optimal operation problem by decomposing the multi-energy system into a subsystem of conversion devices and a subsystem of renewables and

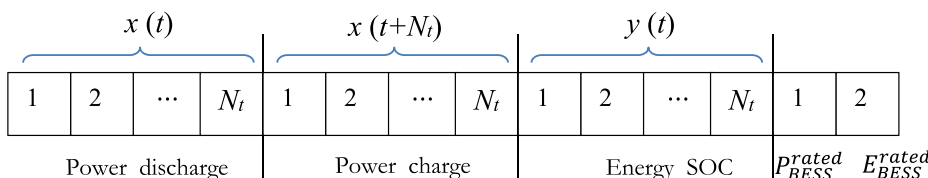


Fig. 9. Schematic of decision variables of optimal design and operation of the BESS.

storage. The MINLP problem was decomposed as a nonlinear programming (NLP) problem and a mixed integer linear programming (MIP) problem, which significantly reduced the computation complexity and set the basis for applying further optimization techniques using the decomposition-coordination strategy. The model was modelled with MATLAB language and solved by *fmincon* solver using the interior-point algorithm, which has an advantage in solving the complex non-linear optimization problem. By defining a set of optimisation variables from the model parameters, the solver was used to determine the set of values that return the minimum value of the objective function. The MATLAB *fmincon* solver was chosen due to its availability as a ready to integrate the authors' combined analysis tool seamlessly. Other Commercial optimization software such as IBM iLog CPLEX, Dash FICO Xpress, GAMS, Gurobi are equally applicable. Parallel computation was adopted to accelerate the converging process, which shortened the running time significantly. In addition, in the configuration of parameters, the precision requirement of the heat network equality constraints ( $10^{-3}$ ) is lower than the electric power flow equality constraints ( $10^{-6}$ ).

## 4. Case study

Data were gathered to apply the model to a real multi-vector district at the University of Manchester (see details in [3]).

### 4.1. Time series input data

The time series input data for electrical and heat loads for each building in electricity and heat networks are known from monitored COHERENT demand data [45], with half hourly resolution. The electrical and heat loads for the buildings in annual peak days as shown in Fig. 10 is taken as exemplificative to run the methodology. The electrical loads at buildings for *one ring main only* (busbars 1–12) was presented. The electrical peak loads occur between 09:00 and 16:00, that is, at times when a university building with teaching and research facilities will reach the higher occupancy levels and usage. The annual load factor is taken as 0.66 [46]. The Manchester district includes heat networks whereby centralized boiler plants deliver heat to multiple buildings (nodes 1–20) through buried pipework.

### 4.2. Scenarios

Energy conversion technologies allow multi-energy exchanges between buildings through the integrated 6.6 kV (13 nodes) electricity network, 85 °C (36 nodes) heat network, and 37 nodes gas network. For heat load, buildings in the district heating network located in area A were supplied by 2 district level conversion devices, other 13 buildings in area B were directly supplied by 13 local gas boilers. The modeled number of devices is equal to the number of existing devices. Utilizing or expanding the heat network with the use of CHP or large scale heat pumps may presents an opportunity for increasing the efficiency of heat and electricity supply to the district. The following scenarios with the variation of conversion devices in supply side were therefore conducted as shown in Table 3. Since gas boilers did not link electricity and heat networks, Scenario 1 was considered as a non-integrated system and was set as a base scenario. Using time series data, the model investigated the impact of a variety of technology options to the electrical, heat and gas networks.

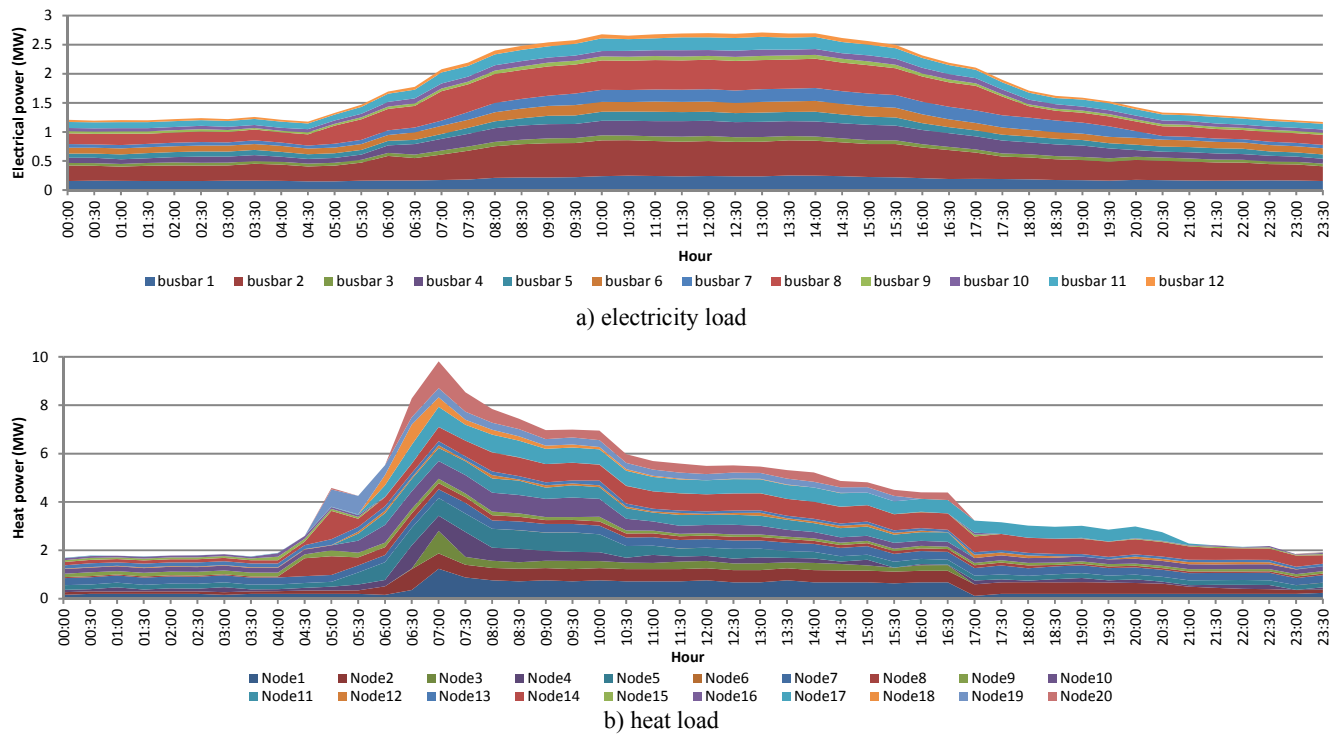


Fig. 10. Building loads in electrical and heat networks in annual peak days for this case study.

**Table 3**  
Scenarios with the various conversion devices at district levels.

	District-level supply for area A	+	Building-level supply for area B
Scenario 1 (base)	District level gas boilers	+	Local gas boilers
Scenario 2	District level CHP	+	Local gas boilers
Scenario 3	District level heat pumps	+	Local gas boilers

**Table 4**  
Energy prices, carbon footprints and carbon price.

Year	Natural gas price (p/kWh)	Carbon footprints (gCO <sub>2</sub> /kWh)		Carbon price (£/tonne)
		Grid electricity	Natural gas	
2016	1.18 (34.6pence/therm)	370	225–330	22.38
2030	2.11 (61.84pence/therm)	100	225–330	36.11

**Table 5**  
Costs and other parameters used for district level conversion devices.

Flexible heating options		Gas fired Boilers	Gas turbine CHP	Large Heat Pumps
CAPEX	Fixed	42.6£/kW <sub>h</sub>	533£/kW <sub>e</sub>	497£/kW <sub>e</sub>
O&M Cost	Fixed (£/MW/year)	1420	14,200	1420
	Variable (£/MWh)	0.78	3.91	5.96
Efficiency (or COP)		91%	34%	350%
Heat-to-power ratio		N/A	1/0.71	N/A
Economic service life (years)		25	25	25

**Table 6**  
Input data with an impact on the optimization of the battery coupled with PV.

Battery cost (kW, kWh)	\$209/kWh in 2017 [11]
Grid electricity price	3-tier TOU tariff [47]
PV electricity export price	4.85 p/kWh [44]
PV peak power full load hours	990 h [50]
PV generation profile	See [52]
Load profile	See Fig. 10
PV and battery economic lifetime	20 years, 15 years [54]
Discount factor	4% [56]

### 4.3. Financial data

#### 4.3.1. Market data

The UK economy 7 tariff is a two-tier time-of-use tariff, one for 7 h off-peak period and the other hours for the peak period. It could be seen that the off-peak tariff is about 6.03 p/kWh between the 7 h (23:00–7:00). The peak is charged at about 16.24 p/kWh between the other hours (7:00–23:00) [44]. Recently, the first three-tier TOU tariff was launched in the UK by Green Energy. This tariff is known as ‘TIDE’, and on April 2018 its three tiers are an overnight off-peak rate of 6.41 p/kWh between 23:00 and 06:00, an evening peak rate on weekdays only of 29.99 p/kWh between 16:00 and 19:00, and a midpeak rate of 14.02 p/kWh at all other times, as shown in Fig. 15 [47].

Natural gas prices as shown in Table 4 are obtained from National grid using base case data [48]. Carbon price as shown in Table 4 is obtained from National grid using base case data [48], where, 1 therm = 29.3 kWh. The carbon footprints for natural gas and grid electricity is also shown in Table 2 [49]. It has to be highlighted that static emission factors have been applied here for illustrative purposes.

#### 4.3.2. Conversion device data

The costs and other parameters of conversion devices are shown as Table 5 [50]. The unit MW is used both for electric generation capacity and heat production capacity. The size unit of gas boilers was MW<sub>h</sub>, and the size units of CHP units and heat pumps were MW<sub>e</sub>. In Scenario 1, capacities of central gas boilers are 6.2 MW<sub>h</sub> and 4.8 MW<sub>h</sub>. In Scenario

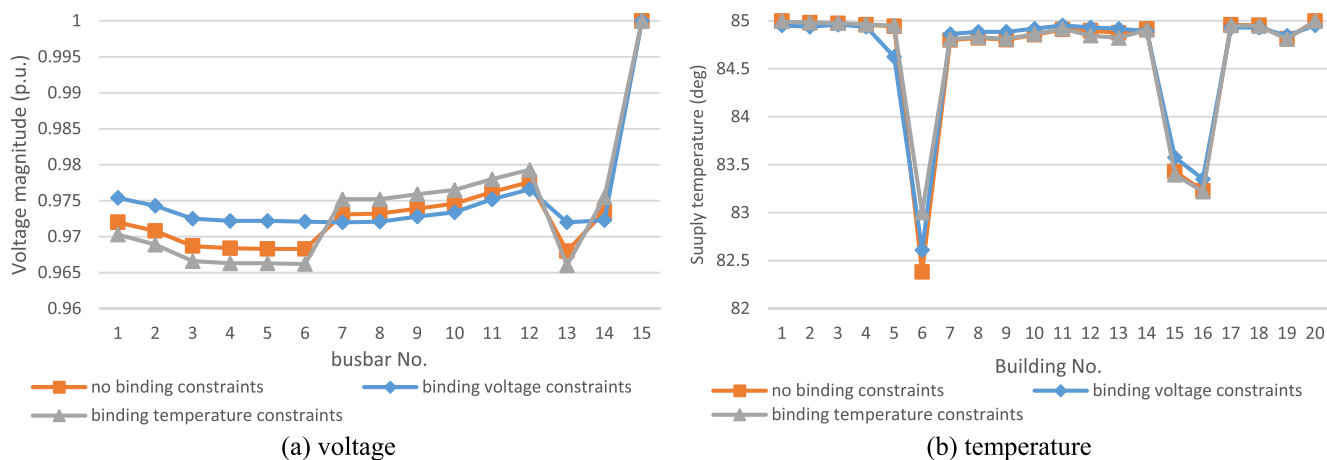


Fig. 11. Voltage at each busbar and supply temperature at each node when a few inequality constraints were binding.

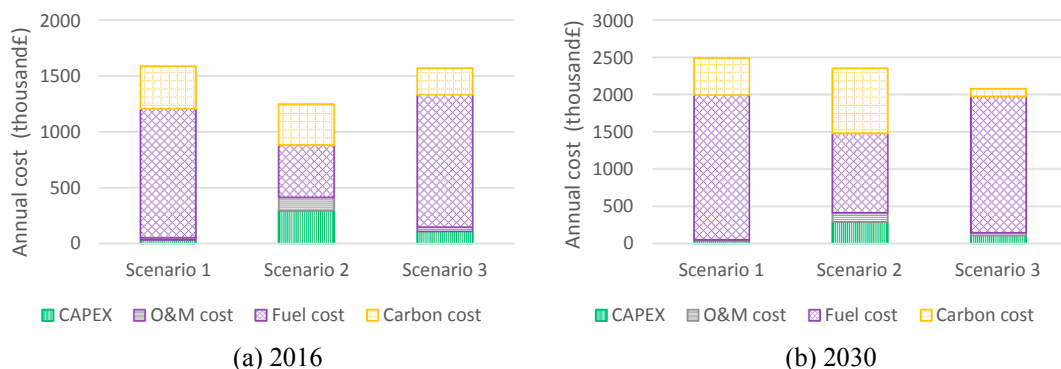


Fig. 12. Breakdown of annual costs of various district level conversion devices in Scenarios 1–3 (units. thousand£).

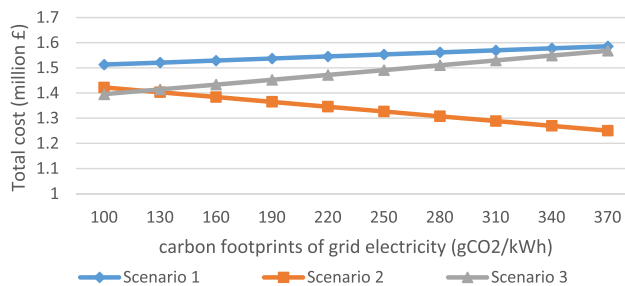


Fig. 13. Comparison of annual total costs for conversion devices in Scenarios 1–3 from a range of grid electricity CO<sub>2</sub> intensity.

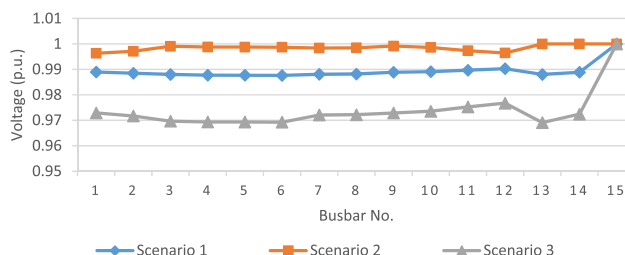


Fig. 14. Voltage magnitudes at each busbar in peak load hour.

2, the district level CHP units are gas turbines with nominal electrical capacity of 5.5 MW<sub>e</sub>. Financial data are all in GBP (£), fixed prices, at the 2015-level and exclude value added taxes (VAT) and other taxes. CHP units and heat pumps have much higher CAPEX and lower OPEX comparing to gas boilers. A tariff is fixed and agreed upon at the time of the contract, where CHP units receive this set amount for each kWh unit

of electricity generated with export tariff is 4.85 p/kWh [51].

4.3.3. PV and battery storage data

Feed-in-Tariffs (FITs) are subsidies received by owners of some low-carbon technologies located in the UK. The FiT scheme includes a generation tariff and export tariff. The generation tariff is paid for every kWh of PV generated and the export tariff is paid for every kWh exported. As an example, a photovoltaic installation in 2017 obtains £0.01915 per kWh [11]. With no battery storage and higher PV generation compared to electricity demand, the PV satisfies onsite demand and the excess PV is sold to the grid at the cheap PV FiT export tariff (4.85 p/kWh) [51]. These data changes do not however affect this paper’s conclusions.

The typical PV daily generation profile was known from [52]. The PV generation at each hour was scaled by a same value for the case study. The useful life of the PV system is assumed to be 20 years, a conservative estimate [53]. The PV investment cost is 1.314£/W in 2015. The PV peak power full load hours is 990 h [50]. The total annual PV generation was calculated as the PV full load hours multiplied by the nominal capacity of PV  $990P_{PV}^{rated}$ .

The cycle stability of the lithium-ion-based battery system is set at 5000 cycles with charge/discharge efficiency 95%. Battery storage technologies are assumed to be maintenance free and to have a lifetime of 15 years [54]. BNEF’s lithium-ion battery price index shows a fall from \$1000 per kWh in 2010 to \$209 per kWh in 2017. Lithium-ion battery pack prices will drop to \$96 per kWh in 2025 and further drop to \$70/kWh by 2030 [55].

Input data with an impact on the optimal sizing of the battery coupled with PV is shown in Table 6. The sizing of electrification technologies (i.e., heat pumps, etc.) has an impact on the load profile. The larger of the difference of peak and trough prices and the smaller of

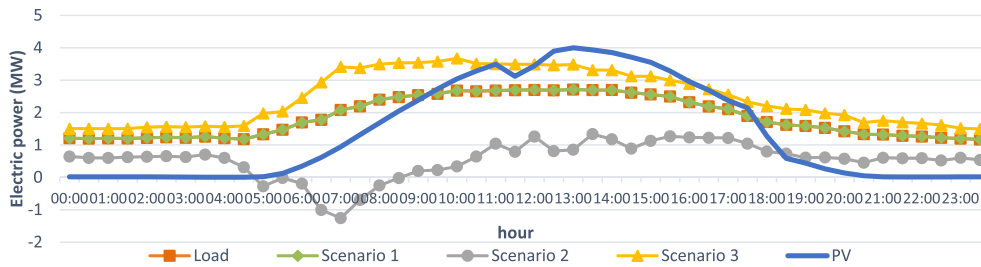


Fig. 15. The profile of load minus the electric power generation of conversion devices in half-hourly time series.

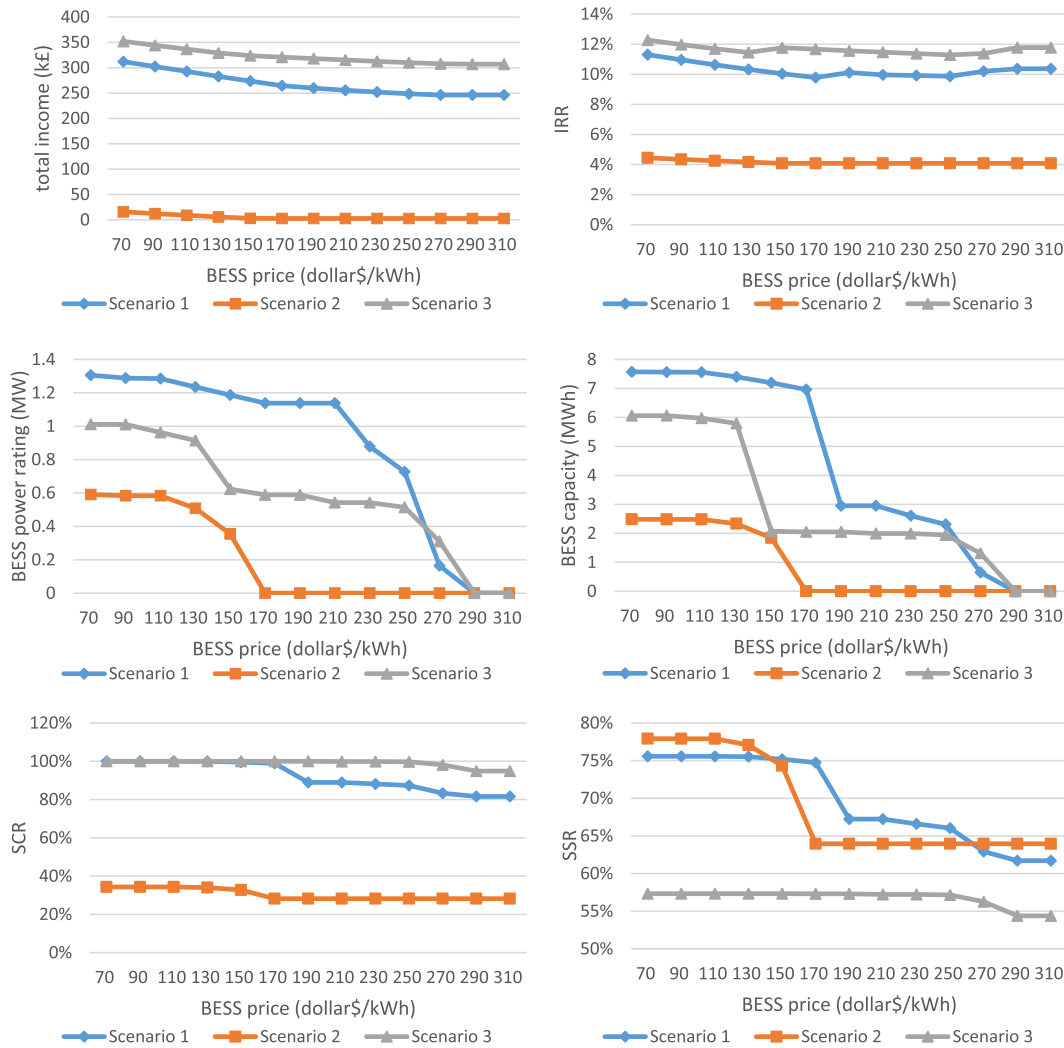


Fig. 16. Optimal sizing of BESS and other indicators with the relation to the BESS price for Scenarios 1–3.

the solar PV export price, the benefit of the battery deployment is better.

## 5. Results

### 5.1. Conversion devices

In different cases of binding inequality constraints, voltage at each busbar and supply temperature at each node in Scenario 3 were shown in Fig. 11. The interactions between the electricity, heat and gas networks through conversion devices were thus clearly demonstrated. No.15 was the busbar connected to the main grid; No.13 and 14 were busbars where the district level conversion devices were located. The low temperatures at building 6, 15 and 16 occurred due to low heat

load, which leads to low mass flow rate and then larger temperature drop. To meet stricter voltage constraints in the electricity network, the temperatures in the heat network may be deteriorated and vice versa. The total operation cost changed accordingly when electrical and thermal network constraints were binding.

The breakdown of annual costs for each scenario were presented in Fig. 12. The impact of energy prices and carbon prices on the option of energy conversion devices was quantified. Without considering carbon prices, the option of CHP was advantageous comparing to other options. Considering carbon prices, the option of CHP was still advantageous using 2016 financial data. However, as the carbon footprint of grid electricity decreases significantly and the carbon price increases notably in 2030, the option of heat pumps is comparably advantageous.

The relation between annualized total costs and carbon footprints of

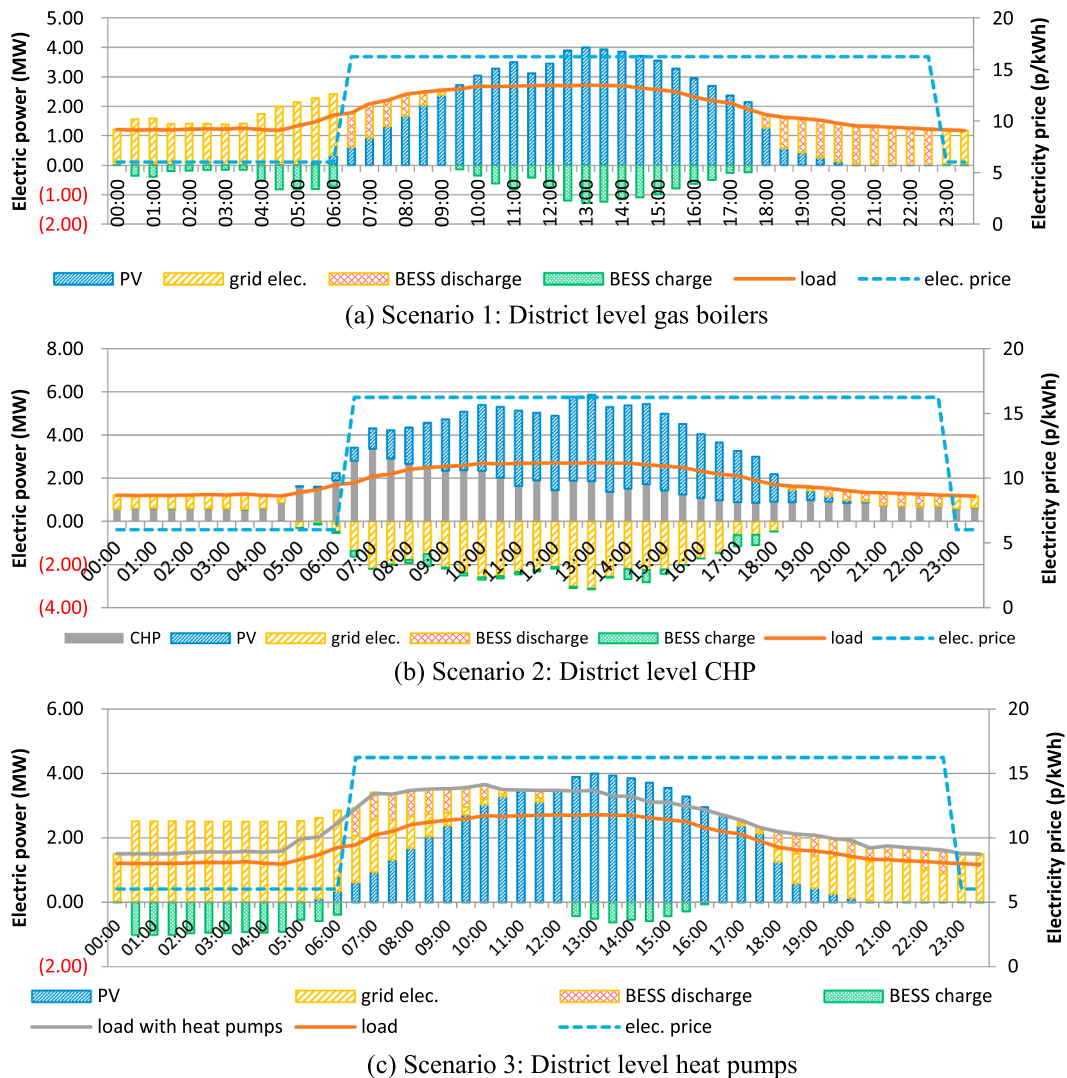


Fig. 17. Electric power balance for typical half-hourly time series.

grid electricity (100–370  $g_{CO_2}/kW$ ) was investigated for Scenarios 1–3 as shown in Fig. 13. It is shown that the total cost of CHP is lower than heat pumps until the grid emissions factor reduces to around 130  $g_{CO_2}/kW$ .

To illustrate the impact of network constraints, voltage magnitudes at each busbar in peak load hour were shown in Fig. 14. The detailed differences in results for the considered Scenarios depend on a number of parameters and multi-energy supply technologies. In particular, by changing local electrical generation (e.g., by CHP) or consumption (e.g., by heat pumps) levels, different effects on voltage and losses profiles, which were key variables in electrical networks, can be appreciated. It is shown that CHP mitigated voltage drop and heat pumps increased voltage drop. The penetration of heat pumps in Scenario 3 led to a noticeable voltage drop to 0.969p.u. In absolute terms, this is not significant and still far from minimum accepted voltage drops for medium voltage distribution networks, which is in the order of 6%, due to the fact that the case study network is very robust. However, it may be expected that for other networks voltage drop may be more significant, and the model is well suitable to capture this while considering interaction with other energy networks too.

Based on the optimal operation of gas boilers, CHP units and heat pumps, the profiles of original electric load minus the electric power generation of conversion devices (adding heat pump consumption or deducting CHP generation) in half-hourly settlement periods in peak

day were simulated in Fig. 15. For better comparison using PV-battery systems, in each scenario one of two district level conversion devices is assumed as district level gas boilers. This paper assessed the impact of the increasing net-load variability on cost optimized PV-battery system design and operation.

### 5.2. PV-battery systems

The optimal capacity of BESS and associated costs with the relation to BESS price were shown in Fig. 16. Here, the total income referred to the reverse of total cost (CAPEX + OPEX). When the BESS price was declined to be less than 150\$/kWh, the income of PV-battery systems was significantly increased due to a notable larger size of BESS installation. The penetration of heat pumps decreased the required optimum battery capacity. The penetration of CHP decreased the required optimum battery capacity. The use of CHP decreased the PV self-consumption ratio (SCR = 0.34), while the use of heat pumps increased the SCR (0.99–1) and decreased the self-sufficiency ratio (SSR) since the electricity load was increased. A larger SCR usually meant a larger internal return rate (IRR). The IRR was much lower in Scenario 2 with CHP since most PV electricity was exported to the grid with lower tariff.

The arbitrage of the battery was from the difference between grid electricity prices when storing electricity and discharging electricity. For PV-battery systems, the surplus PV electricity may be charged to the

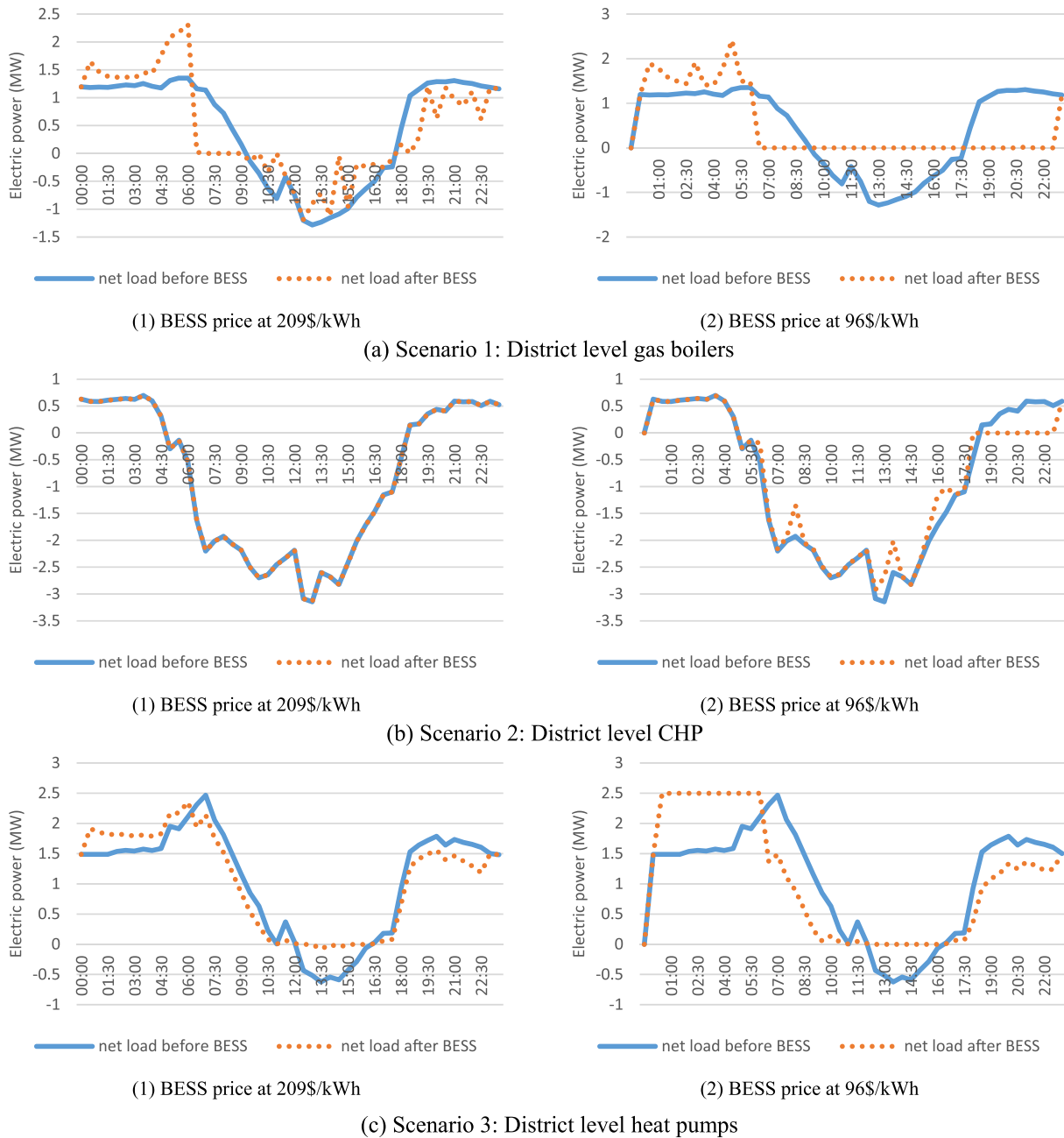


Fig. 18. Impact of BESS on net load under different BESS prices.

battery and then discharged in the evening when there was high demand in the peak price period. The extra benefit of the PV-battery coupling was from the difference of the grid electricity price between the cheap PV FiT export tariff and discharging the stored surplus PV electricity. Increased use of electric heat pumps increased the SCR from the consumption of the mid-day surplus PV and increase arbitrage revenue.

At BESS price 96 \$/kWh, the electric power balance for half-hourly time series was shown in Fig. 17. The histogram showed the amount of electric power balancing by PV, BESS discharging/charging, the grid, CHP and heat pumps. The operation strategy of BESS was charging in the trough price period and in the case of cheap surplus PV power and discharging in the peak price and in the evening with less or no PV.

- In Scenario 1, the surplus PV in mid-day was charged to BESS and this electricity was discharged in the evening.

- In Scenario 2, almost all of the surplus PV electricity in the mid-day was exported since the load in the evening was supplied by CHP.
- In Scenario 3, the majority of surplus PV electricity in the mid-day was consumed by heat pumps.
- A large part of the battery arbitrage in Scenario 1 was to make use of surplus PV electricity otherwise being exported. A large part of the battery arbitrage in Scenario 3 was to make use of peak and trough electricity prices.

At BESS price 209\$/kWh using 2017 data and 96\$/kWh using 2025 prediction data, the impact of BESS on net load with PV were shown in Fig. 18. At BESS price 209\$/kWh, the peak load (7:00–23:00) was shaved at some extent. At BESS price 96\$/kWh, the BESS effectively smoothed the load curve to zero during the peak period. At other hours, the peak net load may increase due to the battery charging power. However, the charging is organized by setting an upper demand limit

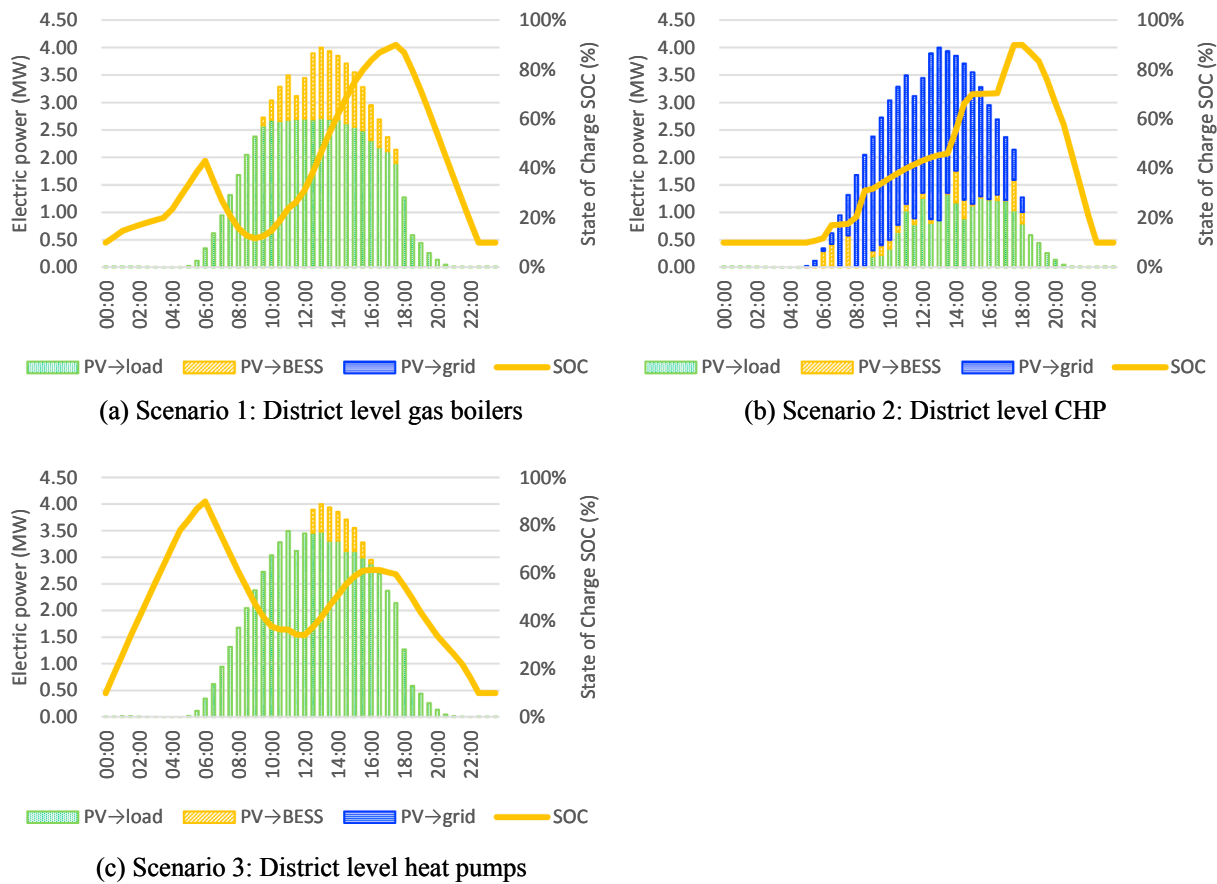


Fig. 19. Energy flow from the PV and the SOC of BESS.

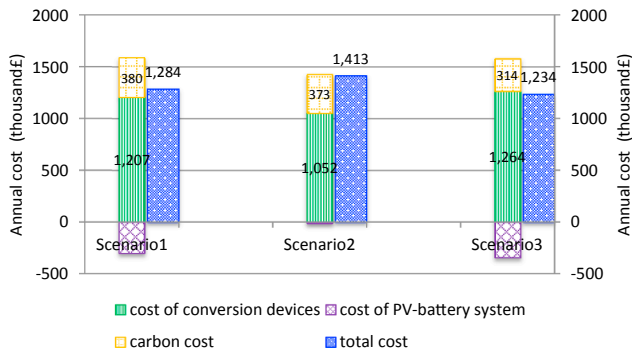


Fig. 20. Breakdown of annual total costs of energy storage and conversion devices in Scenarios 1–3 (units: thousand£).

on the grid. The charging rate plus the load may not exceed this limit, i.e., 2.5 MW in this case.

The energy flows from the PV and the SOC of BESS are shown in Fig. 19. In Scenario 2 with CHP, most of PV electricity is exported to the grid (PV → grid) and thus the SSR is high. In Scenario 3 with a district level heat pump, most of PV electricity is supplied to the load directly (PV → load) and thus the SCR is high. The State of Charge (SOC) graph shows that the BESS in Scenario 1 is mainly charged using the mid-day surplus PV, and the BESS in Scenario 3 is mainly charged using off-peak electricity. The priority of energy flow from PV is: 1. PV → load, 2. PV → BESS, 3. PV → grid. When the PV electricity is surplus for the load, the program optimizes the proportion of PV electricity charged to BESS and exported to the grid.

The total annual costs of all storage and conversion devices for each scenario using 2016 financial data were presented in Fig. 20, which is

equal to the total annual cost of conversion devices minus the annual profit of PV-battery systems. In the optimal operation of PV-battery systems, one of two district level conversion devices in each scenario was assumed as a district level gas boiler. While two district level conversion devices were both CHP units or heat pumps in Section 5.1 for better illustrating the impact of voltage and other operational variables. Fig. 20 showed that after subtracting the profit of PV-battery systems, Scenario 2 with CHP was not advantageous comparing to other options using 2016 financial data. Considering carbon prices, Scenario 3 with heat pumps was advantageous. In conclusion, considering PV-battery systems and the declining grid electricity carbon intensity, the option of heat pumps turned out to be advantageous and may be a favorable option in the long term since heat pumps generally improved the SCR and the profit of the PV-battery system. Furthermore, the PV-battery system mitigated the electricity network infrastructure enforcement caused by heat pumps.

## 6. Conclusions

This paper built a whole-system optimal coordinated operation model of comprehensive storage and conversion devices in multi-vector energy communities. Comprehensive energy storage and conversion devices as well as detailed multi-network energy flows were modelled using matrix formulation, and then decomposed into two subsystems and sequentially optimized. The objective was to minimize OPEX including fuel cost, O&M cost and carbon cost. To meet stricter voltage constraints in the electricity network, the temperatures in the heat network may be deteriorated and vice versa. The total operation cost changed accordingly when electrical and thermal network constraints were binding.

The impact of energy prices and carbon prices on energy conversion

devices was quantified. Without considering carbon prices, CHP was advantageous comparing to other options. Considering carbon prices, CHP was still advantageous using 2016 financial data. However, as the carbon footprints of grid electricity decreasing significantly and the carbon price increasing notably in 2030, the option of heat pumps maintains comparably advantageous. It is shown that total cost of CHP is lower than heat pumps until the grid emission factor reduces to around  $130\text{g}_{\text{CO}_2}/\text{kW}$ .

The income of PV-battery systems was significantly increased when the BESS price is declined to a certain point due to a notable larger size of BESS installation. Due to the relatively high storage costs of batteries, direct PV self-consumption was the major impact factor on total costs. BESS technologies facilitating self-consumption of excess solar PV generation was demonstrated. The benefit of the PV-battery system is to shift off-peak electricity, consume or shift surplus PV electricity, which is influenced by the penetration level of conversion devices. Increased conversion technologies may lead to increased commercial opportunities for energy storage through price arbitrage. Increased use of electric heat pumps increases the PV self-consumption and arbitrage revenue of the PV-battery system.

The option of CHP was advantageous comparing to other options without considering PV-battery systems using 2016 financial data. However, the option of CHP was not advantageous after subtracting the profit of PV-battery systems. It showed that heat pumps with PV-battery systems may be a favorable option in the long term since the grid electricity carbon intensity is declining and heat pumps improve the SCR of PV-battery systems. It showed that for the operation of a multi-energy district, it is of great importance to take into account the interdependency of energy storage and conversion technologies, to

## Appendix A

The Tabs used for input data and the fields of parameter data in the EXCEL spreadsheet are shown in Table 7.

**Table 7**

Tabs for input data and fields of parameter data in the EXCEL spreadsheet.

Electricity network	Heat network	Gas network	Energy conversion device	PV-battery system
Resistance (in <i>per unit, p.u.</i> ) and reactance ( <i>p.u.</i> ) for each line or transformer	Pipe length ( <i>m</i> ), pipe diameter ( <i>m</i> ), roughness ( <i>m</i> ), heat transfer coefficient ( $\text{W m}^{-1}\text{C}^{-1}$ ) for each branch	Pipe length ( <i>m</i> ) pipe diameter ( <i>m</i> )	Electrical efficiency, heat-to-power ratio of CHP, coefficient of performance (COP) for heat pumps, thermal efficiency for electric and gas boilers	CAPEX, lifetime, efficiencies of PV and battery, PV capacity
Electrical active power (MW) at each load	Heat power (MW) at each load	Heat load using gas fuel (MW)	Numberings of conversion devices in electrical, heat and gas networks	Time-of-use price
Voltage at generators, power factors of loads and generators	Supply temperature ( $^{\circ}\text{C}$ ) at each source return temperature ( $^{\circ}\text{C}$ ) at each load		Gas and grid electricity prices, carbon footprints, carbon prices, CHP electricity export price	PV export price, PV peak power full load hours
Electrical load time series at specific locations	Heating load time series at specific locations			PV generation profile

## References

- [1] Heinen S, Hewicker C, Jenkins N, McCalley J, Malley MO, Pasini S, et al. Unleashing the flexibility of gas: innovating gas systems to meet the electricity system's flexibility requirements. *IEEE Power Energy Mag* 2017;15:16–24.
- [2] Liu X, Wu J, Jenkins N, Bagdanavicius A. Combined analysis of electricity and heat networks. *Appl Energy* 2016;162:1238–50.
- [3] Liu X, Mancarella P. Modelling assessment and Sankey diagrams of integrated electricity-heat-gas networks in multi-vector district energy systems. *Appl Energy* 2016;167:336–52.
- [4] Uddin K, Gough R, Radcliffe J, Marco J, Jennings P. Techno-economic analysis of the viability of residential photovoltaic systems using lithium-ion batteries for energy storage in the United Kingdom. *Appl Energy* 2017;206:12–21.
- [5] Parra D, Swierczynski M, Stroe DI, Norman SA, Abdon A, Worlitschek J, et al. Interdisciplinary review of energy storage for communities: challenges and perspectives. *Renew Sustain Energy Rev* 2017;79:730–49.
- [6] Berrueta A, Heck M, Jantsch M, Ursúa A, Sanchis P. Combined dynamic programming and region-elimination technique algorithm for optimal sizing and management of lithium-ion batteries for photovoltaic plants. *Appl Energy* 2018;228:1–11.
- [7] Yang Y, Li H, Aichhorn A, Zheng J, Greenleaf M. Sizing strategy of distributed battery storage system with high penetration of photovoltaic for voltage regulation and peak load shaving. *IEEE Trans Smart Grid* 2014;5:982–91.
- [8] Khalilpour R, Vassallo A. Planning and operation scheduling of PV-battery systems: a novel methodology. *Renew Sustain Energy Rev* 2016;53:194–208.
- [9] McKenna E, Pless J, Darby SJ. Solar photovoltaic self-consumption in the UK residential sector: new estimates from a smart grid demonstration project. *Energy Policy* 2018;118:482–91.
- [10] Linssen J, Stenzel P, Fleer J. Techno-economic analysis of photovoltaic battery systems and the influence of different consumer load profiles. *Appl Energy* 2017;185:2019–25.
- [11] Mariaud A, Acha S, Ekins-Daukes N, Shah N, Markides CN. Integrated optimisation of photovoltaic and battery storage systems for UK commercial buildings. *Appl Energy* 2017;199:466–78.

- [12] McKenna E, McManus M, Cooper S, Thomson M. Economic and environmental impact of lead-acid batteries in grid-connected domestic PV systems. *Appl Energy* 2013;104:239–49.
- [13] Pimm AJ, Cockerill TT, Taylor PG. The potential for peak shaving on low voltage distribution networks using electricity storage. *J Storage Mater* 2018;16:231–42.
- [14] Yu D, Liu H, Yan G, Jiang J, Le Blond S. Optimization of hybrid energy storage systems at the building level with combined heat and power generation. *Energies* 2017;10:606.
- [15] Mashayekh S, Stadler M, Cardoso G, Heleno M. A mixed integer linear programming approach for optimal DER portfolio, sizing, and placement in multi-energy microgrids. *Appl Energy* 2017;187:154–68.
- [16] Zhang D, Shah N, Papageorgiou LG. Efficient energy consumption and operation management in a smart building with microgrid. *Energy Convers Manage* 2013;74(Oct):209–22.
- [17] Acha S, Mariaud A, Shah N, Markides CN. Optimal design and operation of distributed low-carbon energy technologies in commercial buildings. *Energy* 2018;142:578–91.
- [18] Noussan M, Jarre M, Roberto R, Russolillo D. Combined vs separate heat and power production – primary energy comparison in high renewable share contexts. *Appl Energy* 2018;213:1–10.
- [19] Zhou Z, Zhang J, Liu P, Li Z, Georgiadis MC, Pistikopoulos EN, et al. two-stage stochastic programming model for the optimal design of distributed energy systems. *Appl Energy* 2013;103:135–44.
- [20] Li Z, Xu Y. Optimal coordinated energy dispatch of a multi-energy microgrid in grid-connected and islanded modes. *Appl Energy* 2018;210:974–86.
- [21] Good N, Mancarella P. Flexibility in multi-energy communities with electrical and thermal storage: a stochastic, robust approach for multi-service demand response. *IEEE Trans Smart Grid* 2019;10:503–13.
- [22] Cardoso G, Brouhard T, DeForest N, Wang D, Heleno M, Kotzur L. Battery aging in multi-energy microgrid design using mixed integer linear programming. *Appl Energy* 2018;231:1059–69.
- [23] Omu A, Choudhary R, Boies A. Distributed energy resource system optimisation using mixed integer linear programming. *Energy Policy* 2013;61:249–66.
- [24] Morvaj B, Evins R, Carmeliet J. Decarbonizing the electricity grid: the impact on urban energy systems, distribution grids and district heating potential. *Appl Energy* 2017;191:125–40.
- [25] Ceseña EAM, Mancarella P. Energy systems integration in smart districts: robust optimisation of multi-energy flows in integrated electricity, heat and gas networks. *IEEE Trans Smart Grid* 2019;10:1122–31.
- [26] Geidl M, Andersson G. Optimal power flow of multiple energy carriers. *IEEE Trans Power Syst* 2007;22:145–55.
- [27] Ayele GT, Haurant P, Laumert B, Lacarrière B. An extended energy hub approach for load flow analysis of highly coupled district energy networks: illustration with electricity and heating. *Appl Energy* 2018;212:850–67.
- [28] Liu X. Combined analysis of electricity and heat networks PhD Thesis Cardiff University; 2013.
- [29] Liu X (2019-03-17). Input data in Excel spreadsheet Available: [https://www.researchgate.net/publication/331824016\\_inputdata\\_dimmer\\_APEN20190317xlsx](https://www.researchgate.net/publication/331824016_inputdata_dimmer_APEN20190317xlsx).
- [30] Weedy BM, Cory BJ, Jenkins N, Ekanayake JB, Strbac G. *Electric power systems*. 5th ed. Wiley; 2012.
- [31] Grainger JJ, Stevenson WD. *Power system analysis*. (New York): McGraw-Hill; 1994.
- [32] Weisstein EW. Permutation matrix. From MathWorld—A Wolfram Web Resource. <http://mathworld.wolfram.com/PermutationMatrix.html>.
- [33] Luthander R, Widén J, Nilsson D, Palm J. Photovoltaic self-consumption in buildings: a review. *Appl Energy* 2015;142:80–94.
- [34] Barros JA, Leite H. Coordinating independent non-dispatchable generation and energy storage systems. *Int J Electr Power Energy Syst* 2014;62:212–20.
- [35] Ameli H, Qadrdan M, Strbac G. Value of gas network infrastructure flexibility in supporting cost effective operation of power systems. *Appl Energy* 2017;202:571–80.
- [36] Fazlollahi S, Becker G, Maréchal F. Multi-objectives, multi-period optimization of district energy systems: III. Distribution networks. *Comput Chem Eng* 2014;66:82–97.
- [37] Li F. Spatially explicit techno-economic optimisation modelling of UK heating futures PhD Thesis UCL Energy Institute, University College London; 2013.
- [38] Zhang X, Strbac G, Teng F, Djapic P. Economic assessment of alternative heat decarbonisation strategies through coordinated operation with electricity system – UK case study. *Appl Energy* 2018;222:79–91.
- [39] Rees MT, Wu J, Jenkins N, Abeysekera M. Carbon constrained design of energy infrastructure for new build schemes. *Appl Energy* 2014;113:1220–34.
- [40] US Department of Energy (2018/11/28). The importance of flexible electricity supply. Available: <https://www1.eere.energy.gov/solar/pdfs/50060.pdf>.
- [41] Kirschen DS, Strbac G. *Fundamentals of power system economics*. 2nd ed. Wiley; 2018.
- [42] Zheng M, Wang X, Meinrenken CJ, Ding Y. Economic and environmental benefits of coordinating dispatch among distributed electricity storage. *Appl Energy* 2018;210:842–55.
- [43] Beck T, Konziella H, Huard G, Bruckner T. Assessing the influence of the temporal resolution of electrical load and PV generation profiles on self-consumption and sizing of PV-battery systems. *Appl Energy* 2016;173:331–42.
- [44] Sani Hassan A, Cipcigan L, Jenkins N. Optimal battery storage operation for PV systems with tariff incentives. *Appl Energy* 2017;203:422–41.
- [45] Coherent Research Ltd. (18.09.2018). Available: <https://www.ems.estates.manchester.ac.uk/DCS/Logon.aspx?ReturnUrl=%2fDCS>.
- [46] Ma J, Silva V, Belhomme R, Kirschen DS, Ochoa LF. Evaluating and planning flexibility in sustainable power systems. *IEEE Trans Sustain Energy* 2013;4:200–9.
- [47] Pimm AJ, Cockerill TT, Taylor PG. Time-of-use and time-of-export tariffs for home batteries: effects on low voltage distribution networks. *J Storage Mater* 2018;18:447–58.
- [48] National Grid (2017). 2017 Future Energy Scenarios. Available: <http://www2.nationalgrid.com/UK/Industry-information/Future-of-Energy/Future-Energy-Scenarios/>.
- [49] Postnote. Carbon Footprint of Heat Generation. The Parliamentary Office of Science and Technology; 2016.
- [50] Danish Energy Agency (2017, Technology Data for Energy Plants. ([2018-05-01]). Available: [https://ens.dk/sites/ens.dk/files/Analyser/technology\\_data\\_catalogue\\_for\\_energy\\_plants\\_-\\_aug\\_2016\\_update\\_oct\\_nov\\_2017.pdf](https://ens.dk/sites/ens.dk/files/Analyser/technology_data_catalogue_for_energy_plants_-_aug_2016_update_oct_nov_2017.pdf).
- [51] OFGEM (2018-06-17). Feed-in-Tariffs (FIT): Generation & Export Payment Rate Table 01 April – 30 June 2016. Available: <https://www.ofgem.gov.uk/environmentalprogrammes/fit/fit-tariff-rates>.
- [52] Richardson I, Thomson M, Infield D, Clifford C. Domestic electricity use: a high-resolution energy demand model. *Energy Build* 2010;42:1878–87.
- [53] Bertsch V, Geldermann J, Lühn T. What drives the profitability of household PV investments, self-consumption and self-sufficiency? *Appl Energy* 2017;204:1–15.
- [54] Beck T, Konziella H, Huard G, Bruckner T. Optimal operation, configuration and sizing of generation and storage technologies for residential heat pump systems in the spotlight of self-consumption of photovoltaic electricity. *Appl Energy* 2017;188:604–19.
- [55] BNEF (2018-09-17). Bloomberg new energy outlook 2018. Available: <https://bnf.turtl.co/story/neo2018?teaser=true>.
- [56] Morvaj B, Evins R, Carmeliet J. Optimising urban energy systems: simultaneous system sizing, operation and district heating network layout. *Energy* 2016;116:619–36.